# Pattern regulation in a regenerating jellyfish

**Chiara Sinigaglia[1,2,#,*], Sophie Peron[1,2], Julia Steger[1,#], Evelyn Houliston[1], Lucas Leclère[1,*]**

1. Sorbonne Université, CNRS, Laboratoire de Biologie du Développement de Villefranche-sur-mer (LBDV), 06230 Villefranche-sur-mer, France.

2. These authors contributed equally to this work.

# Present address: CS: Institut de Génomique Fonctionnelle de Lyon (IGFL), École Normale Supérieure de Lyon, CNRS UMR 5242 - INRA USC 1370, 69364 Lyon cedex 07, France; JS: Department for Molecular Evolution and Development, Centre of Organismal Systems Biology, University of Vienna, Vienna A-1090, Austria.

*For correspondence: chi.sinigaglia@gmail.com, lucas.leclere@obs-vlfr.fr.

**Abstract**

How body pattern is redefined to allow appropriate restoration of lost parts is a fundamental question in regenerative biology. Jellyfish, with their tetraradial symmetry, offer an unexplored paradigm for addressing patterning mechanisms during regeneration. Here we show that the extensive regenerative capacities of *Clytia* jellyfish do not rely on an actively maintained global patterning system, but instead emerge from local interactions. Any major injury triggers an actomyosin-powered remodeling process that restores body umbrella shape, repositions structures and generates hubs of rearranged radial smooth muscle fibers. These hubs define the position for feeding organ blastema formation. Growth of the feeding organ then requires both cell proliferation and long-range cell recruitment; its morphogenesis is directed by local interactions with the gastrovascular canal system. Such patterning systems, in which mechanically-driven remodeling precisely positions blastema formation, might represent a widespread feature of regenerating animals.

**Keywords:** self-organization, regeneration, wound-healing, stem cell, jellyfish, Cnidaria, Hydrozoa, *Clytia hemisphaerica,* muscle, symmetry.

## Introduction

Regrowth of new structures and their integration into existing body parts during animal regeneration require varying contributions from cell proliferation and tissue remodeling, an issue already highlighted by early studies on planarians (Morgan, 1901). The (re)specification of positional information has been largely attributed to organizer-like centers and gradients of diffusible morphogens, modeled to pattern the surrounding cells in a concentration-dependent manner (eg. (French et al., 1976; Lander, 2013; Raz et al., 2017; Witchley et al., 2013). In planarians, hydra polyps or vertebrates, the site of injury transforms into a signaling center resetting positional information and triggering the regrowth of missing elements through proliferation and/ or tissue remodeling (Chera et al., 2009; Owlarn et al., 2017). Alongside morphogen-based systems, structural and mechanical cues can also contribute to patterning. Supra-cellular actin fibers, for instance, mechanically direct the orientation of body axis during regeneration of hydra polyp fragments (Livshits et al., 2017).

Cnidarians, the sister group of bilaterian animals, display remarkable regenerative capacities. So far, studies of regeneration have mainly focused on the polyp stage of the cnidarian life cycle, rather than the medusa stage, a sexually reproductive, dispersive form generated asexually from the polyp in many species of the medusozoan clade (Leclère et al., 2016). As well as *Hydra* polyps, which are a classic regeneration model (Galliot, 2012), the colonial hydrozoan *Hydractinia* (Bradshaw et al., 2015; Gahan et al., 2016) and the sea anemone *Nematostella vectensis* (Amiel et al., 2015; DuBuc et al., 2014; Schaffer et al., 2016) have become valuable systems for studying wound healing and whole-body regeneration.

Compared to the polyp stage, medusae (= jellyfish) display complex tissue architectures, including striated muscles and well-defined organs, and thus offer an attractive system for studying both whole organism repatterning and organ restoration. In scyphozoan jellyfish the regenerative capacity seems relatively limited; a recent study showed that lost parts are not replaced in juveniles following amputation, although rotational symmetry is restored by a simple muscle-powered process termed “symmetrization” (Abrams et al., 2015). Hydrozoan jellyfish, however, possess greater developmental plasticity than scyphozoans (Hargitt, 1899, 1903; Morgan, 1899; Neppi, 1918; Schmid, 1974; Schmid and Alder, 1984; Schmid and Tardent, 1971). The pioneering work of V. Schmid and P. Tardent provided an initial characterization of the regenerative capacity of hydrozoan medusae, including the ability of wild-caught *Clytia hemisphaerica* to reconstitute organs and restore umbrella shape after diverse types of damage (Schmid, 1974; Schmid et al., 1976; Schmid and Tardent, 1971). *Clytia* is now a reliable laboratory model with extensive genomic and transcriptomic resources (Houliston et

al., 2010; Leclère et al., 2019) amenable to gene function analysis (Momose et al., 2018). *Clytia* medusae show four-fold rotational symmetry around the feeding organ, called manubrium (**Figure 1A-C**). The distribution of elements within the medusa can thus be defined by positional values along a radial axis (i.e. from the umbrella center to the rim), and angular spacing (**Figure 1B**). We can distinguish four identical morphological units, called quadrants, each comprising a portion of umbrella harboring one radial gastrovascular canal, a gonad, one lobe of the tetraradially organized manubrium (**Figure 1D**) and a segment of the circular peripheral canal connecting the tentacle bulbs (up to four per quadrant). The manubrium, tentacle bulbs and gonads harbor populations of stem cells (Denker et al., 2008; Leclère et al., 2012), have autonomous functions and can be regarded as true organs. The umbrella is constituted mainly by an acellular connective layer, the mesoglea (**Figure 1C**), and its internal and external surfaces have different properties. The external surface, the exumbrella, is covered by a simple monolayer of epithelial cells (Kamran et al., 2017), while the inner, concave subumbrella is more complex, being composed of three overlapping tissues layers (**Figure 1C**). Within the subumbrella, an endodermal epithelium is in contact with the mesoglea, and is covered by radially oriented smooth epitheliomuscular cells ("radial smooth muscles"), while at the umbrella periphery a further layer of circularly-oriented striated epitheliomuscular cells which power swimming contractions is interposed between the two (**Figure 1C**) (Leclère and Röttinger, 2016).

We employed cutting and grafting experiments to define the patterning rules that govern *Clytia* medusa regeneration and to investigate the underlying cellular mechanisms. Distinguishable phases of wound healing, tissue remodeling and cell proliferation sequentially contribute to the restoration of shape and missing organs. When the central manubrium is lost, tissue remodeling defines its position of regrowth in a predictable manner. Actomyosin-driven wound constriction triggers the remodeling of umbrella tissues, causing the formation of a transient landmark, a "hub" of radial smooth muscle fibers. Stabilized hubs predict the site where a new manubrium will regenerate. We also show that both proliferating stem cells and digestive cell types mobilized from other organs fuel the manubrium anlage, while radial canals locally dictate its geometry. Pattern in regenerating *Clytia* medusae thus emerges from the integration of local interactions between structural elements and long-range recruitment of cells. Based on our findings, we propose an actomyosin-based "spoke and hub" patterning system, which translates the wound-induced remodeling process into a precisely located blastema.

## Results

### Restoration of medusa form involves both regrowth of organs and body remodeling

In order to gain insight into the self-organizing properties of the *Clytia* jellyfish, we explored its regenerative responses by designing a diverse array of dissections (**Figure 1E-J, 1-S1, 1-S2**). Firstly, targeted ablations demonstrated that all organs (feeding manubrium, gonads, tentacle bulbs) and radial canals can fully regenerate (**Figure 1E-H**). Functional manubria regenerated in 4 days (**Figure 1E;** n: 43/44), while gonads (bearing mature gametes) and tentacle bulbs reformed in about a week (**Figure 1F,G, 1-S2**; gonads: 48/48, bulbs: 45/52; after 8 days in fed jellyfish). Removed segments of radial canals rapidly reformed, re-growing from the stumps in both centripetal and centrifugal directions (**Figure 1H**; notice the growing tip). The recovery efficiency of gonads and tentacle bulbs varied, both within and between medusae. It appeared to be affected by the physiological state of the animal, in particular by feeding levels (**Figure 1-S2C,D**). In contrast, the manubrium recovered reliably and stereotypically, suggesting that the feeding organ is prioritized during the regeneration process (**Figure 1-S2E**).

Secondly, a series of diverse cuts of the jellyfish umbrella allowed us to define the parameters of shape restoration (**Figure 1I,J, 1-S1**). Fragments began remodeling rapidly, reducing the wounded surface, and usually restoring the circular jellyfish shape within 24 hours, irrespective of the starting topology and of the number of remaining organs or canals (**Figure 1I, 1-S1**). This is well illustrated by halved ("bisected") jellyfish or quarter fragments, which morph rapidly into a circular, smaller, umbrella (**Figure 1I, 1-S1C,D**). Taken together, the responses to the array of cut topologies indicated that: i) existing organs and canals are largely conserved, ii) the peripheral circular canal determines the final perimeter of the restored umbrella, iii) the final umbrella size correlates with the amount of tissue in the fragment (**Figure 1-S1**). A rare failure in shape restoration concerned medusae from which the entire umbrella margin had been removed (**Figure 1J, 1-S1T)**: these fragments sealed into a spherical shape and died shortly after (**Figure 1J, 1-S1T**). In cases where the manubrium was injured, the organ rapidly sealed before regaining its feeding function (**Figure 1-S1C**). In manubrium-free fragments, cells accumulated at the injured ending of the remaining radial canal(s) within 24 hours post dissection (hpd), and this mass regenerated into a new functional manubrium within 4 days post-dissection (dpd) (**Figure 1I, 1-S1D,M,R**). A minority of manubria sprouted additional radial canals (6/16 of bisected jellyfish showed a third radial canal after 6 weeks, **Figure 1-S1C**).

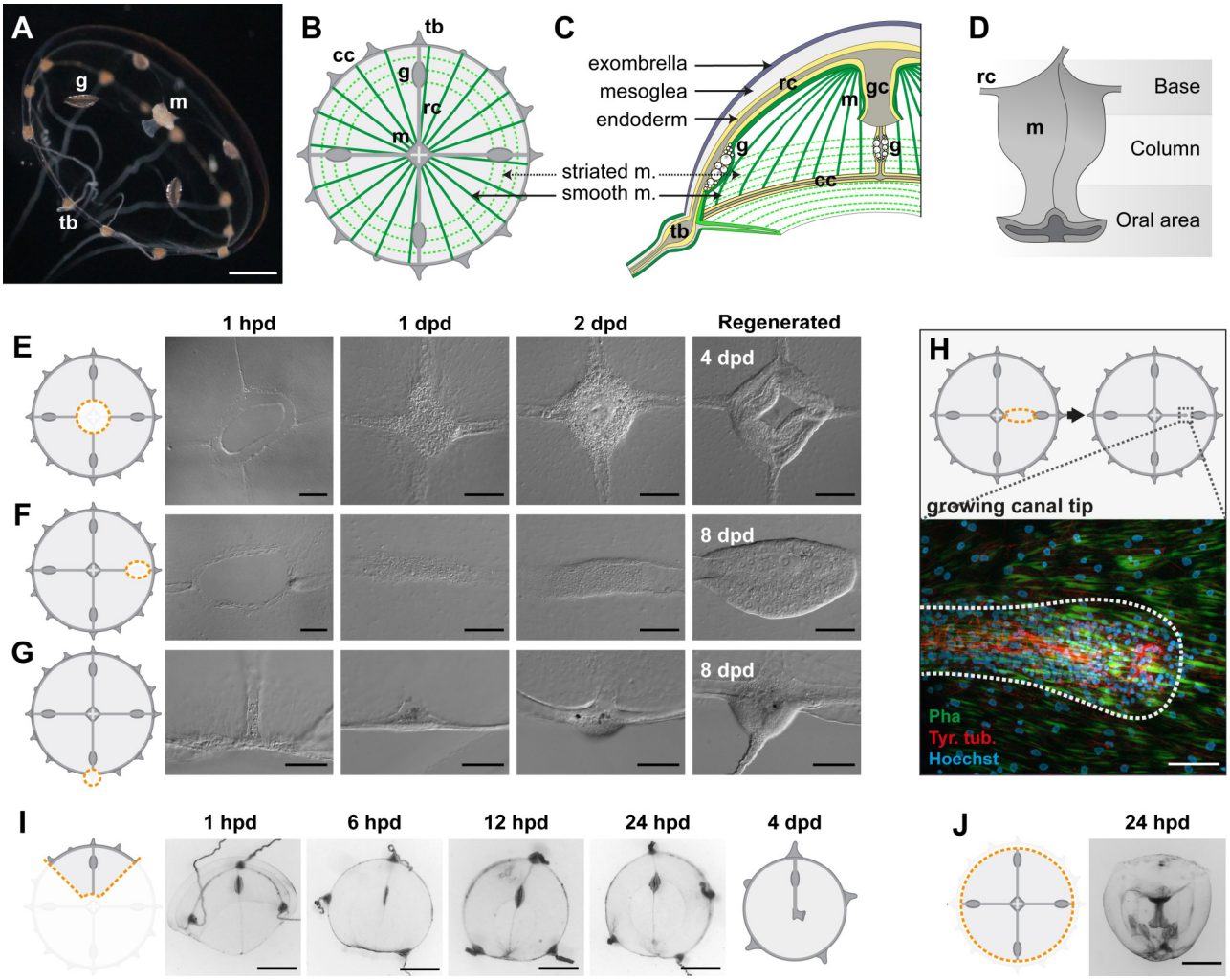


**Figure 1 – Regenerative potential of *Clytia hemisphaerica* jellyfish. (A-D)** Anatomy of *Clytia* medusa. **A)** Female medusa, exumbrellar view. **B)** Tetraradial body organization: each umbrella quadrant comprises a radial canal (rc), a gonad (g), and up to four tentacle bulbs (tb). The tetraradially shaped manubrium (m) lies at the center. A peripheral circular canal (cc) connects the tentacle bulbs. Radial smooth muscle fibers (smooth m.) and circular striated muscle (striated m.) line the subumbrellar layer. **C)** The umbrella comprises an epithelial exumbrella layer, a connective mesoglea, and a subumbrella layer, constituted by endoderm and two layers of muscle fibers (smooth and striated). **D)** Diagram of a manubrium, oral (distal)-aboral (proximal) view. The base comprises four gastric pouches, connected to the four radial canals. The oral area (lip) is organized into four folds. **(E-J)** Regenerative potential of *Clytia* medusa. **E)** Manubrium regenerates in 4 days, **F)** gonads and **G)** tentacle bulbs in 8 days. **H)** Radial canals efficiently regenerate. Detail of the growing tip, showing nerves in the canal (tyr-Tub antibody, shown in red). **I)** Quarter medusa fragment morphs within 24 hours into a smaller medusa, and regenerates a new manubrium in 4 days. **J)** Any type of wound to the umbrella is readily repaired, with the exception of the excision of the entire bell margin, which leads to the medusa fragment sealing on itself without proceeding further with regeneration. Scale bars: A,I-J: 1 mm; E-G: 100 µm; H: 20 µm.

These observations highlighted the strong capacity for tissue and organ repair in *Clytia* jellyfish, but also showed that the final layout of body parts in regenerates does not necessarily match the original topology. Most obviously, missing radial canals were not restored, and the spacing between remaining canals and gonads was unbalanced in many cases (e.g. **Figure 1-S1H,I,P**). Thus restoration of the characteristic tetraradial symmetry of the medusa, manifested by the regular angular

spacing of the organs and canals (see Introduction and **Figure 1B**) is dependent on the elements retained in the regenerate.

**Cell proliferation is required for manubrium regeneration, but not for wound closure or umbrella remodeling**

Following manubrium ablation (**Figure 1E**), the wounded exumbrellar and subumbrellar layers curled and fused together, sealing off the exposed mesoglea (stage 0, *wound closure*). The hole in the umbrella started to constrict progressively, pulling together the cut ends of the four radial canals. By 12 hpd the tissue gap was closed, and the radial canals joined at the center (stage 1, *remodeling*). Cells started accumulating at the junction of the radial canals, the first sign of organ regeneration; by 24 hpd the cell mass formed a roughly square, flat primordium (stage 2, *regeneration primordium*). The primordium thickened, and by 48 hpd it fissured centrally, revealing the now distinguishable gastric cavity (stage 3, *opening*). A thicker rim emerged, which developed into a short tubular outgrowth (stage 4, *outgrowth*). The protuberance elongated, and within 4 dpd, it developed the characteristic lip folds, tetraradially arranged; the manubrium was now fully functional, albeit smaller than the original one (stage 5, *folding*) (**Figure 1-S2F,G**).

The contribution of cell proliferation to manubrium regrowth was assessed by one hour incubation with the thymidine analogue EdU (**Figure 2A-C, 2-S1**). Within the first hours following manubrium ablation, cell proliferation levels in the subumbrella decreased, notably within the segment of radial canals lying between gonad and manubrium (termed “MG-segment”; **Figure 2C, 2-S1**). Cell cycling then increased markedly within the manubrium anlage (24 hpd), notably during the thickening phase (between 48 hpd and 72 hpd; **Figure 2A,B**). Cell proliferation within the radial canals increased again around 48 hpd, and peaked during primordium thickening stage (72 hpd), before returning to basal levels at 96 hpd (**Figure 2A,C, 2-S1A,B**). Treatment with the inhibitor of DNA synthesis hydroxyurea blocked manubrium regeneration at a pre-opening stage (stage 2-3), thus establishing the dependency of manubrium outgrowth on cell proliferation (**Figure 2D,E**). After removal of the inhibitor, the regenerative process resumed, and a complete manubrium formed within 3 days (n: 14/20; **Figure 2E**). Conversely, hydroxyurea treatment did not impair wound healing, umbrella remodeling or the repositioning of regenerating manubrium after bisection (**Figure 2G**), consistent with the relatively low number of cells incorporating EdU during these processes (**Figure 2F**).

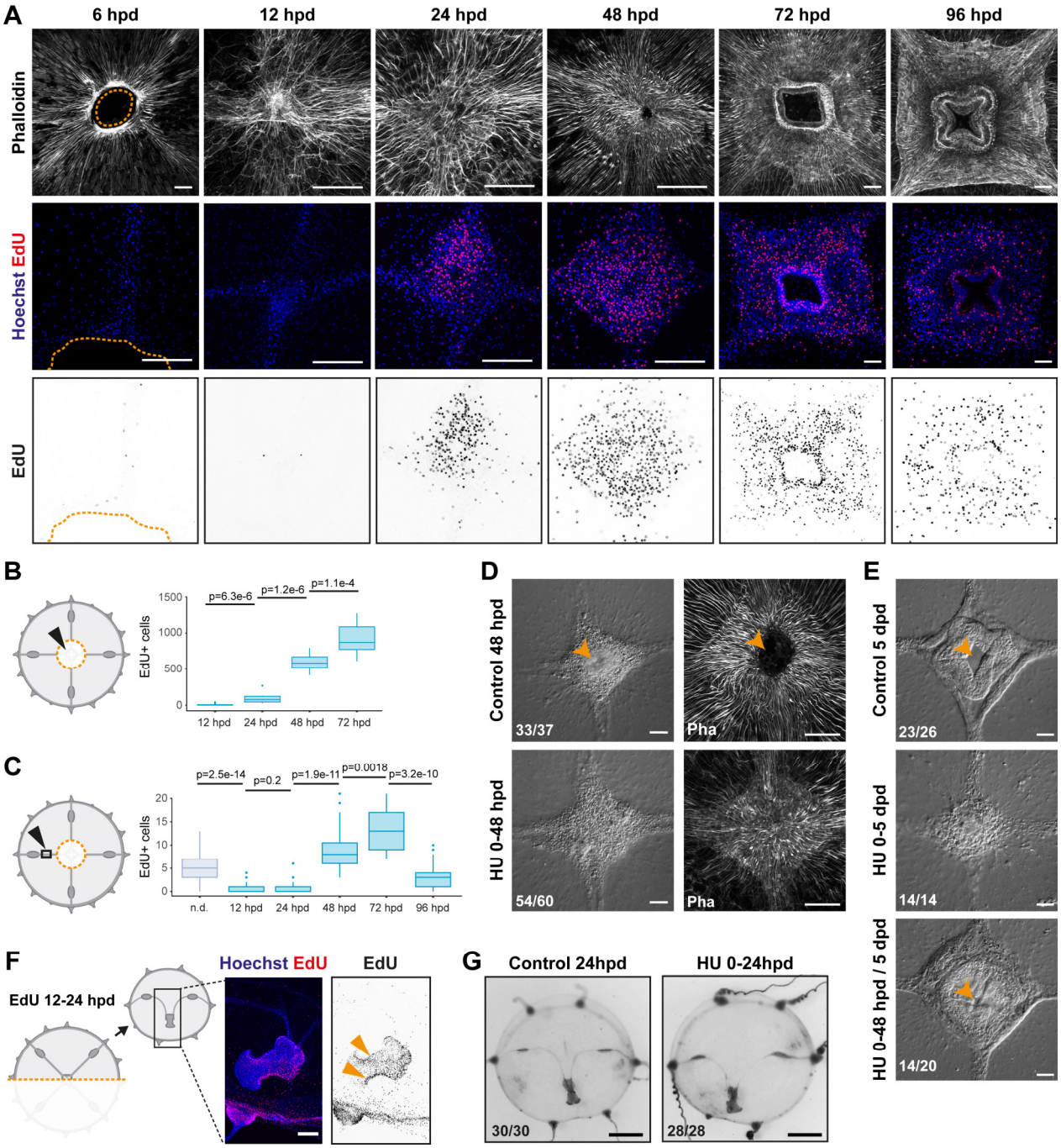


**Figure 2 – Manubrium regeneration, but not umbrella remodeling, requires cell proliferation. (A-E)** Proliferation-dependent manubrium regeneration. **(A,B)** EdU pulse labelling shows that cell proliferation strongly increases in the manubrium anlage, visualized by phalloidin staining (in white), starting from 24 hpd (quantification shown in **B**). Columns in the panel displays different channels of the same image, except for the first one, where a magnification is shown for second and third row. **(C)** Shortly after injury, cell proliferation levels in the radial canals are reduced, and increase again 48-72 hpd. At 96 hpd proliferation levels return to basal level. n.d.: non dissected. **(D)** Treatment with hydroxyurea (HU) shows that cell proliferation is not necessary for the initial cell mass accumulation (0-48 hpd). **(E)** Cell proliferation is necessary for the manubrium outgrowth, and the correct formation of lobes. Removal of HU restores proliferation and manubrium morphogenesis. **(F, G)** Remodeling does not require cell proliferation. **F)** EdU pulse shows cycling cells in the proximity of the remodeling margin, but **G)** HU-treatment demonstrates that proliferation is not necessary for successful shape restoration. Scale bars: A,D-F: 100 µm, G: 1 mm. Statistical test: p values calculated with the Mann Whitney Wilcoxon test.

## Cell recruitment via the radial canals sustains manubrium morphogenesis

The high numbers of EdU-labelled cells detected within radial canals during primordium formation (**Figure 2A,C, 2-S1A,B**) raised the possibility that cells are recruited from other parts of the medusa through the canal system. Gonads and tentacle bulbs, which connect to the manubrium via the radial canals, harbor niches of multipotent stem cells (Denker et al., 2008; Leclère et al., 2012) called interstitial stem cells (i-cells; **Figure 3A, 3-S1A**). Hydrozoan i-cells can generate both somatic and germ cell types, and express stem cell markers including *Nanos1* (Bosch, 2009).

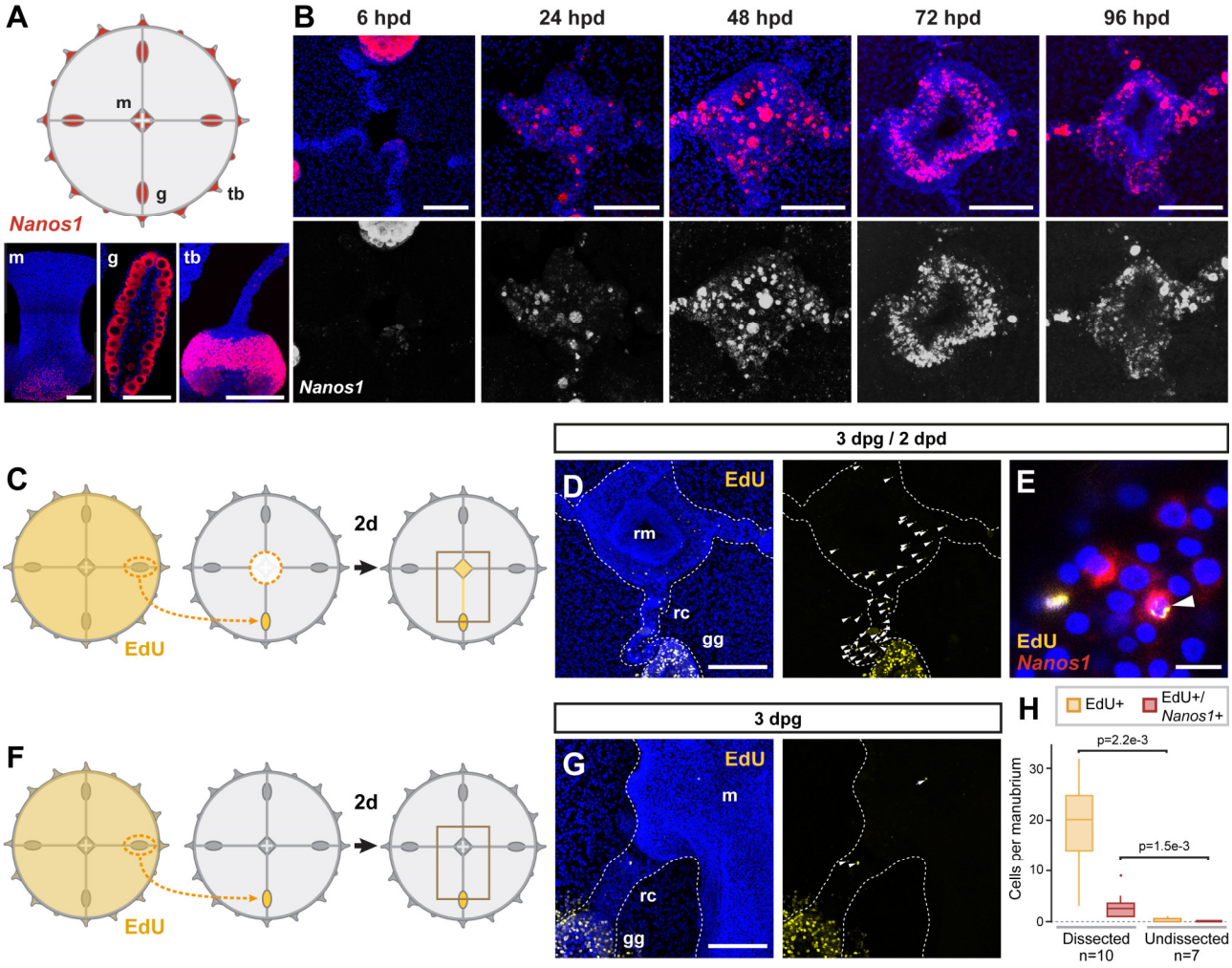


**Figure 3 – Dynamics of i-cell migration during manubrium regeneration. (A)** *CheNanos1*-expressing i-cells (shown in red, detected by FISH) are located at the base of the manubrium, in the gonads and in the ectoderm of tentacle bulbs. **(B)** I-cells, identified by the expression of *CheNanos1*, are also detected in the regenerating anlage and in the radial canals, from 24 hpd. **(C-G)** Grafting experiments demonstrate that stem cells migrate from the gonad to the site of manubrium regeneration. **C)** Diagram of experimental approach: a donor medusa is incubated with EdU for 24 hours, one gonad is then excised and grafted at the place of one of the gonads of a non-treated receiver. **D)** 48 hours after manubrium dissection, EdU-positive cells are detected in the radial canal connecting the grafted gonad to the regenerating manubrium, and in the manubrium primordium as well (white arrowheads). **E)** A fraction of the EdU-positive cells found in the regenerating manubrium express *CheNanos1* (white arrowhead), indicating that they likely are migrating i-cells. **F)** Diagram of control experiment: an EdU labeled gonad is grafted to a non-regenerating host. **G)** In non-regenerating EdU+ gonad-grafted

animals, none or only few EdU-positive cells can be found the manubrium and the radial canal connected to the grafted gonad, 3 days post graft (white arrowheads; detail of larger image shown in Figure 3-S1G). **H)** EdU-positive and EdU/*CheNanos1* double positive cells are abundant in regenerating manubrium while nearly absent in non-regenerating manubria. Abbreviations: m: manubrium, rm: regenerating manubrium, g: gonad, gg: grafted gonad. tb: tentacle bulb, rc: radial canal. Nuclei are shown in blue. Statistical test: p values calculated with the Mann Whitney Wilcoxon test. Scale bars: A-C,E: 100 µm, D: 10 µm.

In situ hybridization detection of *CheNanos1* revealed i-cells in both regenerating manubrium and radial canals, starting from 24 hpd (**Figure 3B**). We could demonstrate that some of these i-cells came from the gonad by replacing a gonad in a host medusa prior to manubrium ablation with one from an EdU-labeled donor (24 hs incubation with EdU; **Figure 3C, 3-S1B-E**). 48 hours after manubrium ablation, EdU-positive cells were detected in the host medusa both within the regenerating manubrium and in the connecting radial canal (**Figure 3C, 3-S1F-I**), and a subpopulation of those migrating EdU+ cells expressed *CheNanos1* (**Figure 3E,H, 3-S1F-H**). EdU+/*Nanos1*+ cells were found exclusively in the MG-segment of radial canals and in the manubrium primordium (**Figure 3D, 3-S1F-I**), indicating that cell migration from the gonad is directed towards the regenerating manubrium. Unexpectedly, small oocytes labeled with EdU were also detected both in the radial canal and regenerating primordium (**Figure 3B, 3-S1H**); the fate of these oocytes in the primordium is unclear. No mobilization of EdU+/*Nanos1*+ cells from the gonad was observed in undamaged medusae (**Figure 3F-H**), suggesting that recruitment of i-cells and other cell types is specifically triggered by the regeneration process.

We noted that another cell type, characterized by brown pigmentation, circulated actively in the canals during regeneration and appeared to integrate the primordium. In undamaged jellyfish, these cells were located in the endoderm of the manubrium, gonads and tentacle bulbs (**Figure 4A**). These previously undescribed cells, which we term Mobilizing Gastro-Digestive (MGD) cells circulated rapidly within the lumen of the radial canal following manubrium ablation, likely transported by the flagellar beating of canal endodermal cells that govern nutrient flow (**Figure 4C**). We could label them specifically by feeding the medusa with fluorescent beads (**Figure 4A**, see Methods), supporting the idea that they function in nutrient uptake, and that the brown pigmentation derives from the crustacean diet (artemia nauplii). We noted that the MGD cells also mobilized in the radial canals in starvation conditions, albeit less markedly than in regenerating jellyfish (**Figure 4D**), suggesting a role in regulating nutritional balance between organs. Analysis of bead-labeled jellyfish following manubrium dissection revealed that some of the endodermal cells of the regenerating manubrium did indeed originate from other organs of the jellyfish (**Figure 4B**). Transplantation of a gonad from a medusa fed with fluorescent beads to an unlabeled host prior to manubrium ablation confirmed that MGD cells from the gonad endoderm are recruited by the primordium of the regenerating manubrium, as well as by other non-regenerating organs (**Figure 4E**). In medusae from which all gonads had

been removed, fluorescent-bead-labelled MGD were detected in the manubria primordia once the radial canals had regrown, showing that these cells can be recruited not only from the gonad but also from more peripheral regions, likely from the endoderm of the tentacle bulbs (**Figure 4F**). On the other hand, no fluorescent-bead-labelled MGD cells were found in the manubrium primordium if the gonads and the radial canals were completely ablated (**Figure 4F**) demonstrating that MGD travel uniquely though the endodermal canal system.

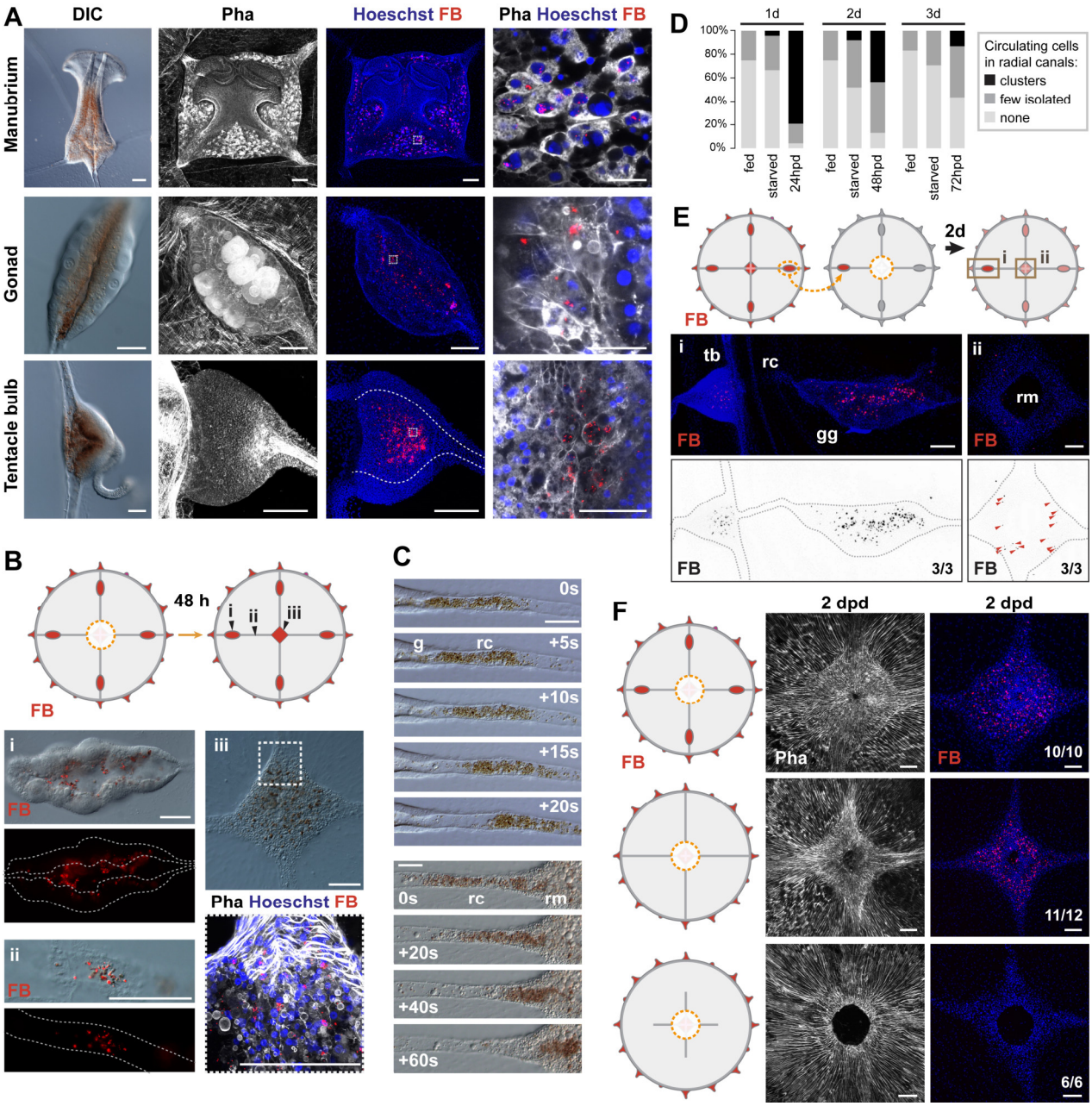


**Figure 4 –Non-targeted cell recruitment of Mobilizing Gastro-Digestive (MGD) cells during regeneration**. **(A)** Cells containing dark products of digestion are embedded in the endoderm of all organs (manubrium, gonads and tentacle bulbs; first column of panel). Fluorescent micro-bead (FB, shown in red) feeding labels these brown-colored cells, and proves their gastro-endodermal nature. **(B)** In manubrium-regenerating medusae, FB-labeled cells are found in the gonad digestive

cavity (i), moving through the radial canals (ii) and accumulating in the regenerating manubrium (iii). **(C)** Time frame of MG-segment showing fast movement of the MGD cells in the lumen of the radial canal (rc), out from the gonad (g, top panels, 0-20 seconds), into the regenerating manubrium (rm, bottom series, 0-60 sec). **(D)** Quantification of circulating cells in the MG-segment of the four radial canals in fed, starved and regenerating jellyfish. Starved and regenerating animals were last fed 8 hours prior to dissection experiment (n: 24 for each condition) **(E)** Grafting of a FB-labeled gonad to a naïve receiver (experimental design shown in diagram) demonstrates that FB-labeled cells migrate in the regenerating anlage of the manubrium (ii, red arrowheads in bottom figure), as well as in the non-regenerating tentacle bulbs. **(F)** FB-labeled cells (shown in red) derive from the endoderm of gonads, but also of tentacle bulbs (central row of panel showing dissection of manubrium and of the four gonads). If there is no connection to another organ (bottom row), manubrium regeneration is stalled, and no FB-labeled cells can be detected. Scale bars: 100 µm.

Related experiments demonstrated that intact radial canals are necessary for manubrium regeneration. The removal of all four radial canals (including gonads), leaving just their most proximal segments intact, either blocked manubrium regeneration at early stages or led to abnormal manubria with incorrect geometry and disrupted morphogenesis, notably lacking the deep folds shaping the four edges of the manubrium column (**Figure 5A**). Correct morphogenesis of a tetraradial manubrium only occurred when at least one radial canal was connected to the peripheral gastrovascular system (**Figure 5B**).

Based on these results we propose that the recruitment of i-cells, MGD cells and possibly other cell types via the canals to the primordium is necessary for correct manubrium regeneration in *Clytia*. Mobilized cells display two trends: stem cells specifically migrate towards the regeneration site, while digestive cells circulate through the canal system and can settle in the endoderm of any organs, including the manubrium regeneration site.

**Radial canals dictate the geometry of the regenerating manubrium**

The tetraradial symmetry of the native manubrium mirrors the global symmetry of undamaged medusae, and is also perfectly restored in regenerating manubria if properly connected to the canal system (see above; **Figure 5J**). In order to explore further the link between manubrium symmetry and the global tetraradial symmetry of the medusa body, we examined the geometry of the regenerated manubrium in the context of different cut topologies.

Bisected and quarter medusa fragments regenerated double- and single- lobed manubria, respectively (**Figure 5C,D**). Furthermore, irrespective of the dissection topology, the number of lobes of the regenerating manubrium always reflected the number of remaining radial canals, such that three radial canals generated a three-lobed manubrium, and so on (**Figure 5C-F**). This pattern might depend either on an underlying system of circular positional information retained within the medusa fragments, or by a signal coming from the canals themselves. To distinguish these possibilities, we systematically removed radial canals from manubrium-ablated (but otherwise undamaged) medusae.

The presence of four canals led in most cases to a tetraradial manubrium, three canals to a trilobate one, two canals a bilobed manubrium, and one canal to a tubular one (**Figure 5G-J**). We conclude that the topology of the regenerating manubrium is determined by the number of connecting canals, which might provide a mechanical or biochemical signal, and/or might materially contribute to the primordium composition by providing migrating cells (**Figure 3,4**). Arguing against the latter option, canal fragments connected to the primordium but not to any other organ were found to be sufficient to direct the geometry of the regenerated manubrium (**Figure 5B**), as long as at least one canal remained connected to a gonad. Canals appear therefore to exert a local influence on the proliferating primordium, whose nature remains to be determined.

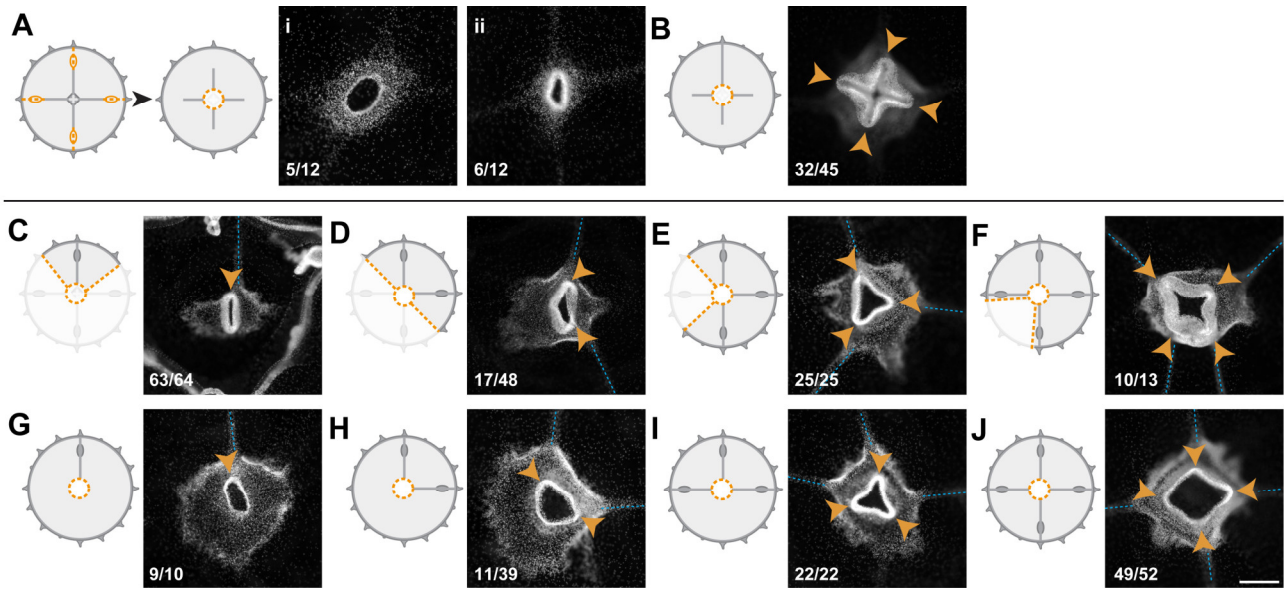


**Figure 5 – Radial canals locally dictate the morphology of regenerating manubrium. (A)** Removal of all four gonads and the peripheral portions of the four radial canals arrests (i) or impairs (ii) manubrium regeneration (6 dpd), showing that correct morphogenesis requires the contribution of radial canals. **(B)** If at least one canal is complete (connected to another organ), morphogenesis is restored. **(C-J)** The geometry of the regenerating manubrium depends on the adjoining radial canals, and not on the global body symmetry. Panels C-F show the removal of entire quadrants, while G-J of gonad/canal systems. **(C, G)** If only a single canal is present, a tubular regenerate will form, independently of the shape of the initial aggregate (manubrium base) and independently of the umbrella symmetry. **(D, H)** Two radial canals entail a bi-lobed (yellow arrowheads) manubrium, irrespective of the umbrella topology; the two lobes follow the angular orientation of canals. **(E, I)** Three-lobed manubrium, connected to three radial canals, and independently of the umbrella topology. **(F, J)** Four radial canals correlate with a tetraradial manubrium. Images show Hoechst staining of regenerated manubria, 6 dpd. Cuts are shown in dark yellow in the diagram; blue dashed lines highlight canals on pictures.

### Muscle fiber ‘hubs’ predict the site of manubrium regeneration

The initial remodeling of fragmented medusae generates a new stable functional state in which circular shape and organ function are recovered. Positional information along the radial axis of the umbrella, from the manubrium site to the rim, is re-established during the remodeling phase, whereas

rotational symmetry depends on local cues. Recovering medusae fragments usually regenerate only one manubrium (see below for an exception), reform radial canals (although not necessarily in the original tetraradial configuration), and regenerate gonads appropriately positioned along the canals. A key question is thus to understand how the position of a new manubrium is determined.

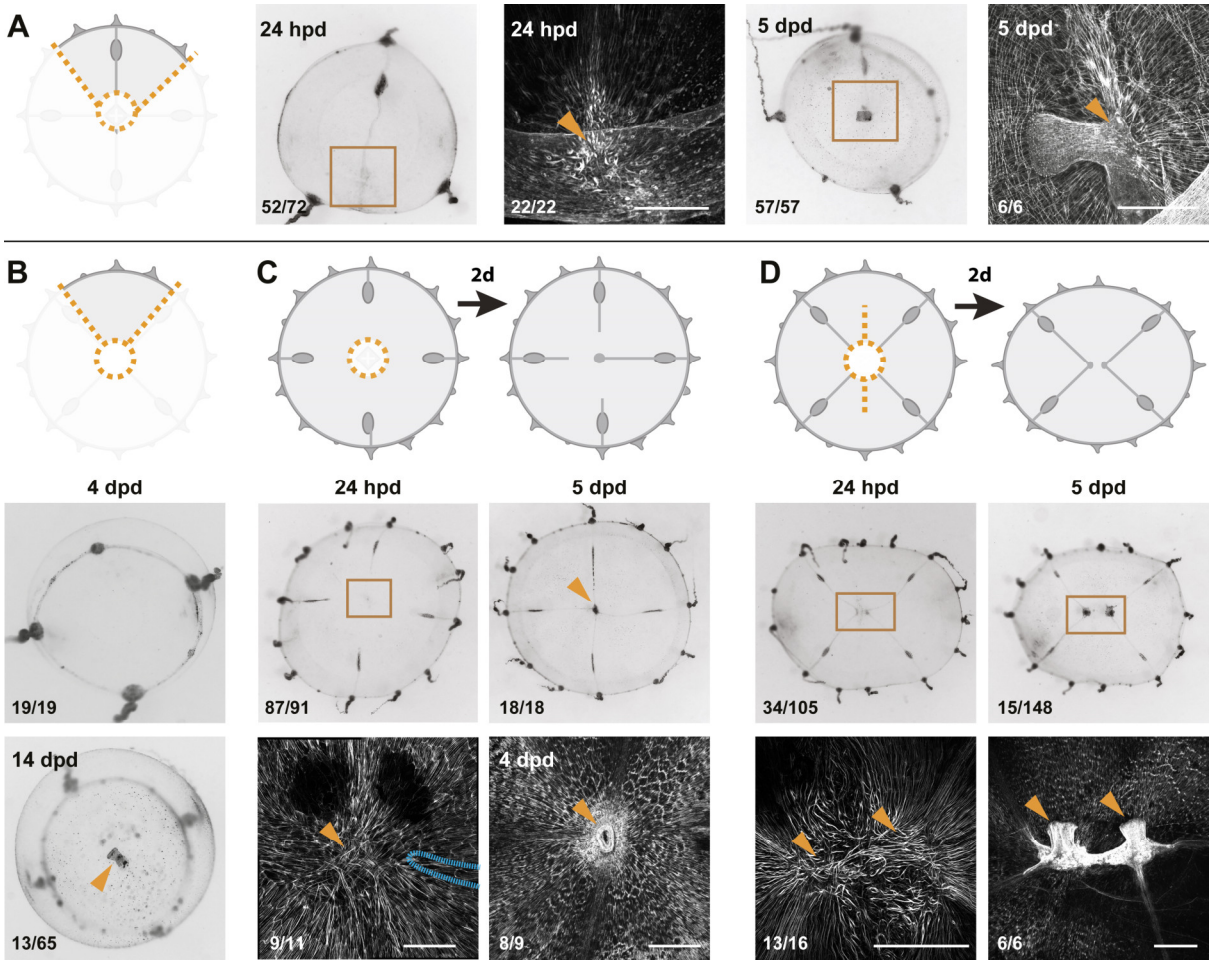


**Figure 6 – Smooth muscle hubs identify the position of regenerating manubria. (A)** Inter-radial quarter dissection: 24 hpd a radially arranged hub of muscle fibers (phalloidin staining) is visible in a location away from the wound site, and close to the injured end of the remaining radial canal. After 5 days, the regenerated manubrium is systematically located at the hub of smooth muscle. **(B)** Umbrella fragments devoid of radial canals can re-circularize, but do not regenerate a manubrium after 4 dpd (top panel). At 14 dpd a small fraction can regenerate a simple tube-shaped manubrium-like structure unable to fed (bottom panel). **(C)** Muscle hub formation does not depend on the presence of radial canals, as shown by the removal of all four canals: in this case, manubrium regeneration (orange arrowhead) is triggered once at least one radial canal (blue dashed line) reaches the muscle hub. **(D)** Inducing the formation of two muscle hubs by a manubrium dissection followed by a longitudinal section of the umbrella leads to the formation of two muscle hubs (orange arrowheads), and later, to two manubria (orange arrowheads) at their precise location. Scale bars: A: 150 µm; C,D: 300 µm.

In undamaged jellyfish, the manubrium is located at the geometrical center of the umbrella, at the point of convergence ('hub') of the radial smooth muscles fibers and of the four endodermal radial canals. The initial position of the regenerating manubrium does not necessarily coincide with the geometrical center of the remodeled medusa (e.g. in quarter jellyfish fragments**; Figure 6A**), while

manubrium anlagen were invariably associated with the radial canal(s) and a hub of smooth muscle fibers. We thus explored whether the canals and/or the smooth muscle fiber hub could contribute to defining the position of the new organ.

Experiments presented above showed that successful manubrium regeneration is dependent on the presence of radial canals. Cells recruited through the radial canals were found to be necessary for correct manubrium morphogenesis (see above: **Figure 5**). Furthermore, interradial fragments lacking a radial canal showed no signs of primordium formation at 4 dpd (**Figure 6B**). After two weeks a simple tube-like manubrium (unable to feed) was observed in a few cases (n: 13/65; **Figure 6B**), showing that umbrella tissues also contribute to the new structure, while canals play a facilitating role by contributing with specific cell types to the blastema. Merging of multiple canal ends (often seen during remodeling, see e.g. **Figure 1-S1**) do not specify the position of manubrium regeneration, as evidenced by quarter jellyfish fragments in which a manubrium regenerated on the sole surviving radial canal (**Figure 6A**).

F-actin staining showed that primordia and regenerated manubria were systematically associated with the hub of smooth muscle fibers that formed during the remodeling process (**Figure 6A**; n: 22/22). In all cases, a muscle hub could be detected before the anlage formed (**Figure 6A, 6-S1B**), irrespective of the wound topology. Hub formation did not require radial canals, since it was unaffected by removal of the MG-segment of radial canals after manubrium excision (**Figure 6C**). In those canal-ablated medusae, manubrium regeneration commenced when at least one of the excised canal regrew to the hub of smooth muscle fibers (**Figure 6C**; primordium on hub (4dpd): 8/9; manubrium at the center of umbrella (5dpd): 18/18). Taken together, these findings suggested that the position of the hub of smooth muscle fibers plays a key role in defining the location of the new organ, while connection to the radial canals fuels primordium growth and morphogenesis.

In order to test the relationship between the muscle fiber hub and the site of manubrium regeneration, we performed a longitudinal deep cut along the umbrella of manubrium-ablated medusae (**Figure 6D, 6-S1D**). This cut topology disrupts the wound closure and remodeling processes, resulting in the formation of two muscle hubs (**Figure 6D**). At 24 hpd, we observed two separate manubrium primordia (**Figure 6D**) that in about a third of cases regenerated two independent manubria, sometimes linked by a radial canal (**Figure 6D**). In other cases, the two manubrium anlagen fused into a single oral structure, correctly patterned or twinned (**Figure 6-S1D**, fused manubria 5 dpd: 24/159). The “double hub” experiments confirmed that i) the formation of a muscle hub is a product of the remodeling process and is independent of the radial canals (**Figure 6C, 6-S1C**), and ii) each hub

marks the location of a regenerating manubrium, irrespective of the subsequent outcome (two manubria or fused; **Figure 6D, 6-S1D**).

**Why does only one manubrium usually regenerate?**

Our initial survey of regeneration capacities showed that any medusa fragment can reform a manubrium (**Figure 1-S1**). This implies that the potential to form a manubrium is present along the entire radial axis of the umbrella (also see (Schmid et al., 1976)) and also that a control mechanism exists that prevent multiple manubria from forming in most cases. One explanation could be that *Clytia* manubrium has an organizing role, as is the case for the hypostome (mouth) of *Hydra* polyps (Bode, 2011; Meinhardt, 1993; Vogg et al., 2019), and provides an inhibitory signal that spreads through the umbrella and prevents the induction of additional manubria. We tested this possibility by grafting supernumerary manubria at different subumbrellar positions. Grafted manubria could co-exist stably with the original one (**Figure 7A**), with each manubrium behaving independently and participating in feeding. The grafted manubria rapidly sprouted new canals, which reconnected to the existing gastrovascular system (**Figure 7A**). In dissected medusae, grafting a fragment of a manubrium base onto the umbrella tissues, either on a radial canal or directly adjacent to the endogenous manubrium, systematically led to the regeneration of a functional extra manubrium (**Figure 7B**; tubular/bi-lobed shape: 12/12). Furthermore, manubria grafted either on the radial canal (**Figure 7C**) or the umbrella (**Figure 7D**) did not prevent the regeneration of an excised manubrium, resulting in the formation of a two-manubrium medusa (n: 10/10 and 17/20, respectively). In contrast, no regeneration occurred when exogenous manubria were grafted adjacent to the excised one (**Figure 7E**; n: 15/20). These experiments indicate that existing manubria can exert a very local inhibition on manubrium reformation.

Examination of muscle fiber organization following manubrium grafting provided a possible explanation for its observed local inhibitory influence (**Figure 7F-H**). Grafted manubria appeared to provoke local reorganization of smooth muscle fibers. Significantly, in cases where the grafted manubria were positioned close to the ablation site of the endogenous manubrium and its regeneration was inhibited, the smooth muscle fibers were not arranged in a hub, irrespective of the presence of canals (**Figure 7H**; n: 11/11). These grafting experiments reinforce the systematic correlation between the presence of a radial muscle hub and the regeneration of a new manubrium. They also allow us to propose that local disturbance of muscle fiber orientation by a grafted manubrium is responsible for inhibiting manubrium regeneration by preventing hub formation.

These experiments indicate that the manubrium itself does not appear to generate a long-range signal affecting organ positioning. The "inhibitory" effect of proximal grafts is likely indirect, and can be explained by a localized rearrangement of the muscle fibers. The manubrium of *Clytia* medusae, unlike the hypostome of *Hydra* polyps, thus does not appear to act as an organizer of global patterning, but can be seen as the pivotal element of a self-organizing system based on local interactions.

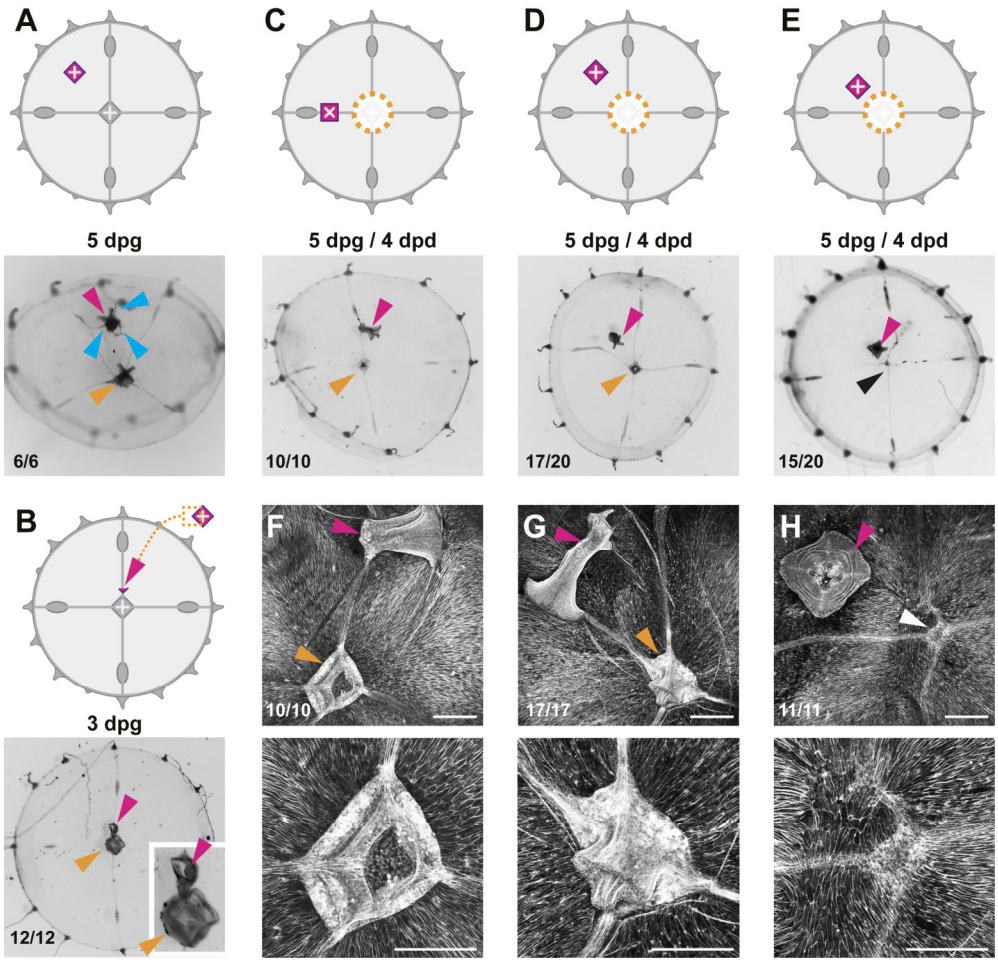


**Figure 7. Effects of additional manubria on manubrium regeneration. (A)** Grafting of an additional manubrium (in purple in the top diagram) on an undissected medusa leads to the formation of a jellyfish with two manubria (purple and orange arrowheads). The grafted manubrium sprouts novel radial canals (blue arrowheads) from its base. Canals will initially grow without apparent directionality, and will connect to the endogenous canal system. (**B)** Grafting of a fragment of manubrium base on the umbrella leads to the regeneration of an extra-manubrium (purple arrowhead)**. (C-E)** Effect of manubrium grafting on manubrium regeneration. If the manubrium is grafted on the radial canal **C)** or in the middle of the umbrella **D)**, it does not inhibit regeneration of the endogenous manubrium (orange arrowhead). **E)** Short-range inhibition (black arrowhead) is observed when the additional manubrium is grafted adjacent to the regeneration site. **(F-H)** The regenerated manubrium is systematically associated with a muscle hub in medusae where the grafted manubrium is either on a radial canal **F)** or on the umbrella **G),** as shown by phalloidin staining. **H)** When regeneration is inhibited, no muscle hub is observed at the junction point of the radial canals. Scale bars: 100 µm.

**Actomyosin-driven subumbrella remodeling restores medusa shape**

Closer examination of the tissue behavior in bisected medusae provided insights into the mechanisms underlying remodeling and shape restoration (**Figure 8**). As for manubrium dissection (**Figure 2A**), the subumbrellar and exumbrellar layers fused together in the first two hours following bi-section, sealing off the mesoglea (**Figure 8A,B**). In the following hours, myoepithelial tissues surrounding the wound site constricted, progressively reducing the cut perimeter (**Figure 8A,B**). This active process of wound closure drew together the intact tissues at each end of the cut edge, restoring the dome-shaped umbrella in less than 24 hours (**Figure 8A,B**). F-actin staining and DiI tracing droplets in the mesoglea demonstrated that umbrella remodeling is accompanied by an extensive reorganization within the area proximal to the wound, of both the subumbrellar radial muscle layer (**Figure 8B,C**) and of the underlying mesoglea (**Figure 8D,E**). During the constriction phase (1 to 12 hpd), tissues and mesoglea adjacent to the wound area were compressed; this correlated with loosening of the radial alignment of the smooth muscle fibers and their partial disorganization (**Figure 8B**, 6 hpd). By 12 hpd, the muscle fibers were still recognizable but appeared heavily distorted by umbrella remodeling. They re-acquired a radial orientation following the repositioning of the manubrium (12-24 hpd) towards the new center of the remodeled medusa (**Figure 8B,C**). Correspondingly, DiI droplets indicated that the mesoglea portion initially close to the wound site surrounded the re-centered manubrium, while distal regions seemed unaffected (**Figure 8D,E**).

A continuous bundle of actin lined the remodeling edge (**Figure 8F**), reminiscent of the actin ring described around wound sites in the exumbrella layer of *Clytia* (Kamran et al., 2017). This bundle resembles the purse-string structures tightening epithelial wounds described in many species, through a contraction of actin/myosin cables stretching over cells at wound edges (Begnaud et al., 2016; Schwayer et al., 2016). Detection of phosphorylation of myosin-II regulatory light chain (MRLC) around the wound area by antibody staining (**Figure 8G**) is consistent with a local activation of the actomyosin contraction system. Actomyosin cables assembled in response to any type of wound in *Clytia* (**Figure 8F, 8-S1C**). Treatment with myosin II inhibitors (Blebbistatin and BDM) impaired umbrella remodeling, providing further evidence that the mechanical forces that underpin remodeling of the umbrella result from actomyosin activity (**Figure 8H, 8-S1A**).

A comparable process described in damaged *Aurelia* ephyrae was proposed to depend on rhythmic contractions of the striated muscles (Abrams et al., 2015), and indeed newly fragmented *Clytia* undergo vigorous contractions (**Figure 8-S1B**). Treatment with the anesthetic menthol, which efficiently blocks umbrella contractions (**Figure 8-S1B)**, did not prevent remodeling of bisected

medusae, inducing only a slight delay of remodeling (**Figure 8I**). This result suggests that in *Clytia* rhythmic contractions of the striated muscle are not necessary to the remodeling process.

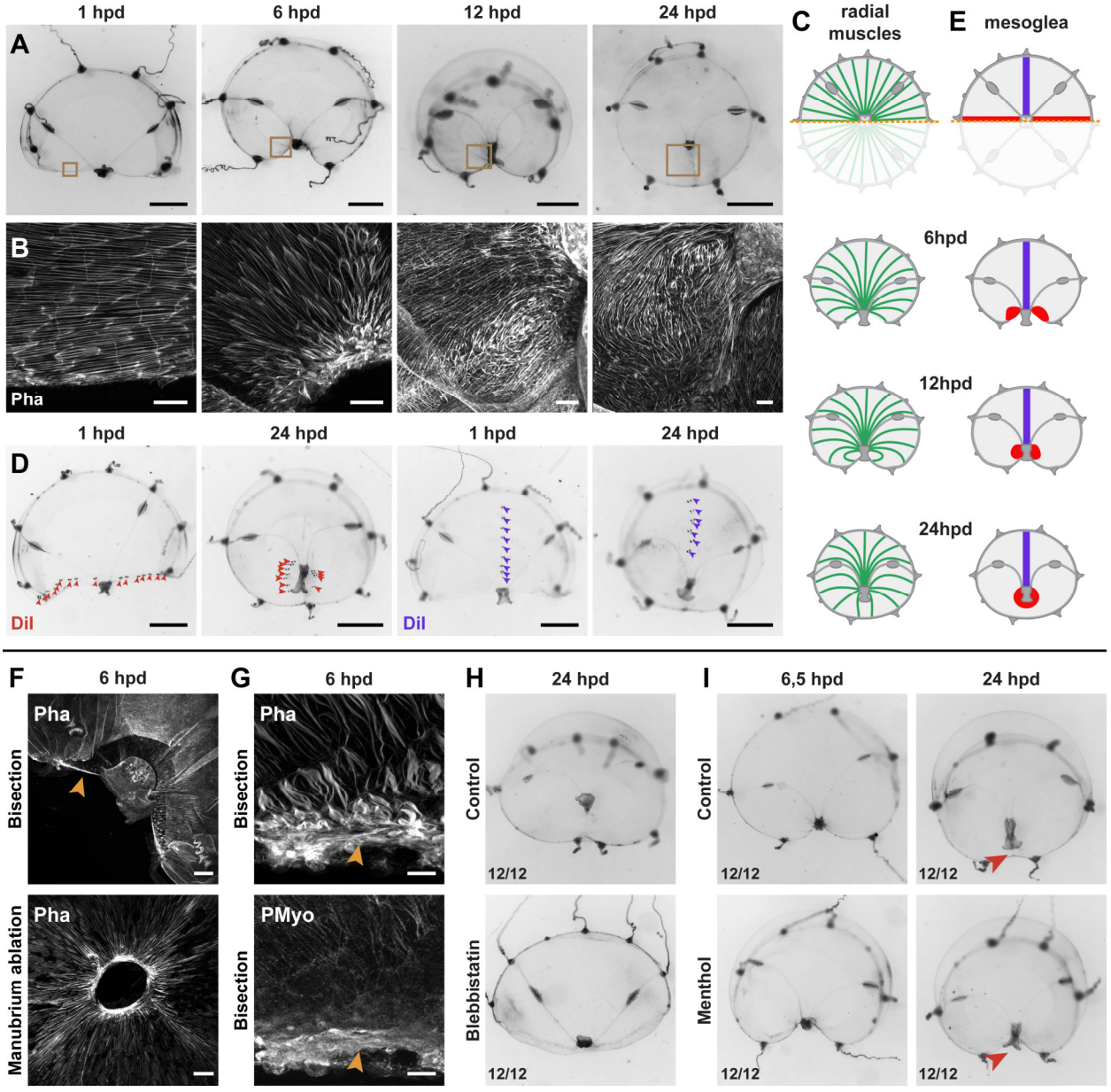


**Figure 8 – Actomyosin-driven subumbrella remodeling restores medusa shape. (A)** Morphology of remodeling hemi-medusa, showing the rapid reduction of exposed edges. After closure of the wound, the manubrium migrates towards the center: by 24 hpd only a scar-like trace is visible in the umbrella, which will then disappear. **(B, C)** Dynamics of muscle fibers at the remodeling edge (phalloidin staining in **B** -corresponding to the brown squares in **A**; diagram in **C**). The initially ordered radial fibers disorganize at the wound edge, and are heavily rearranged following the movements of the umbrella. **(D, E)** Injection of DiI droplets (in **D**) into the thick mesoglea layer of hemi-medusae, along a line following the wound (left images, DiI droplets shown with red arrowheads, n: 8/8 jellyfish) or perpendicular to it (right images, DiI droplets shown with blue arrowheads, n: 6/6 jellyfish). Mesoglea is rearranged close to the wound area, while its more distal region seems unaffected (diagram in **E**). **(F)** Remodeling is driven by an actomyosin cable that assembles at the wound edge in both bisected (top) and manubrium-dissected (bottom) medusae. **(G)** Actin filaments and phosphorylated myosin are strongly enriched at the wound site (orange arrowhead) during remodeling. **(H)** Blebbistatin-based inhibition of myosin II shows that actomyosin is responsible for remodeling. **(I)** Complete inhibition of striated muscle-based rhythmic contractions with menthol (see **Figure 8-S1B**) causes only a minor delay in remodeling (red arrowhead). Scale bars: A,D: 1 mm; F: 50 µm, B,G: 25 µm.

**Hub stabilization is required for manubrium blastema formation**

Actomyosin-driven healing was observed to systematically cause bunching up of smooth muscle fibers. In some cases this bunching configuration became stabilized as a "muscle hub" and was followed by blastema formation. Not every wound, however, induces the regeneration of a new manubrium. To understand how this process is controlled, we performed an asymmetric bisection of the jellyfish umbrella - generating a smaller fragment devoid of manubrium and a larger, manubrium-bearing one (**Figure 9**). In this case, the smaller fragment (S-fragment) regenerates a manubrium, while the larger (L-fragment) does not, an inequality that cannot be attributed to a wound size difference (equal in both fragments) nor, as previously shown (see **Figure 7**), to a long-range inhibitory effect of the existing manubrium. F-actin staining revealed in both fragments a similar initial bunching of injured and disorganizing smooth muscle fibers, close to the healing wound (**Figure 9**). In the S-fragment, smooth muscle fibers started to progressively organize around the hub precursor site, leading to a radial organization of fibers converging on one side towards the "hub", and connected to the margin of the umbrella on the other. This characteristic topology resulted in stabilization of the hub structure, which was maintained during the subsequent re-centering process, and ultimately led to the appearance of a manubrium primordium (**Figure 9A**). In the L-fragment, the severed fibers were also initially gathered into a hub at the wound area (8 hpd). However, they were differently arranged, connected on one side to the wound site and on the other extremity to the manubrium, thus lying parallel (**Figure 9B**). The displacement of this structure away from the wound site (from 10 hpd) led to the local re-orientation of the surrounding fibers, which converged towards the endogenous manubrium (**Figure 9B**). This rearrangement led to the disappearance of the newly formed hub. Consistently, a new manubrium always regenerated in the S-fragments (in correspondence with the hub), but never in an L-fragment.

Taken together, these results suggest that actomyosin-dependent tissue remodeling is the major driver of *Clytia* medusa shape restoration, determining i) the recovery of circular topology, and ii) the formation of the radial smooth muscle hub. Transition to a stable hub in a medusa fragment depends on the configuration of the radial muscle fibers, which ultimately is determined by the wound topology. We suggest that stabilization of the muscle hub can only occur when the fibers are not constrained by attachment to an existing hub.

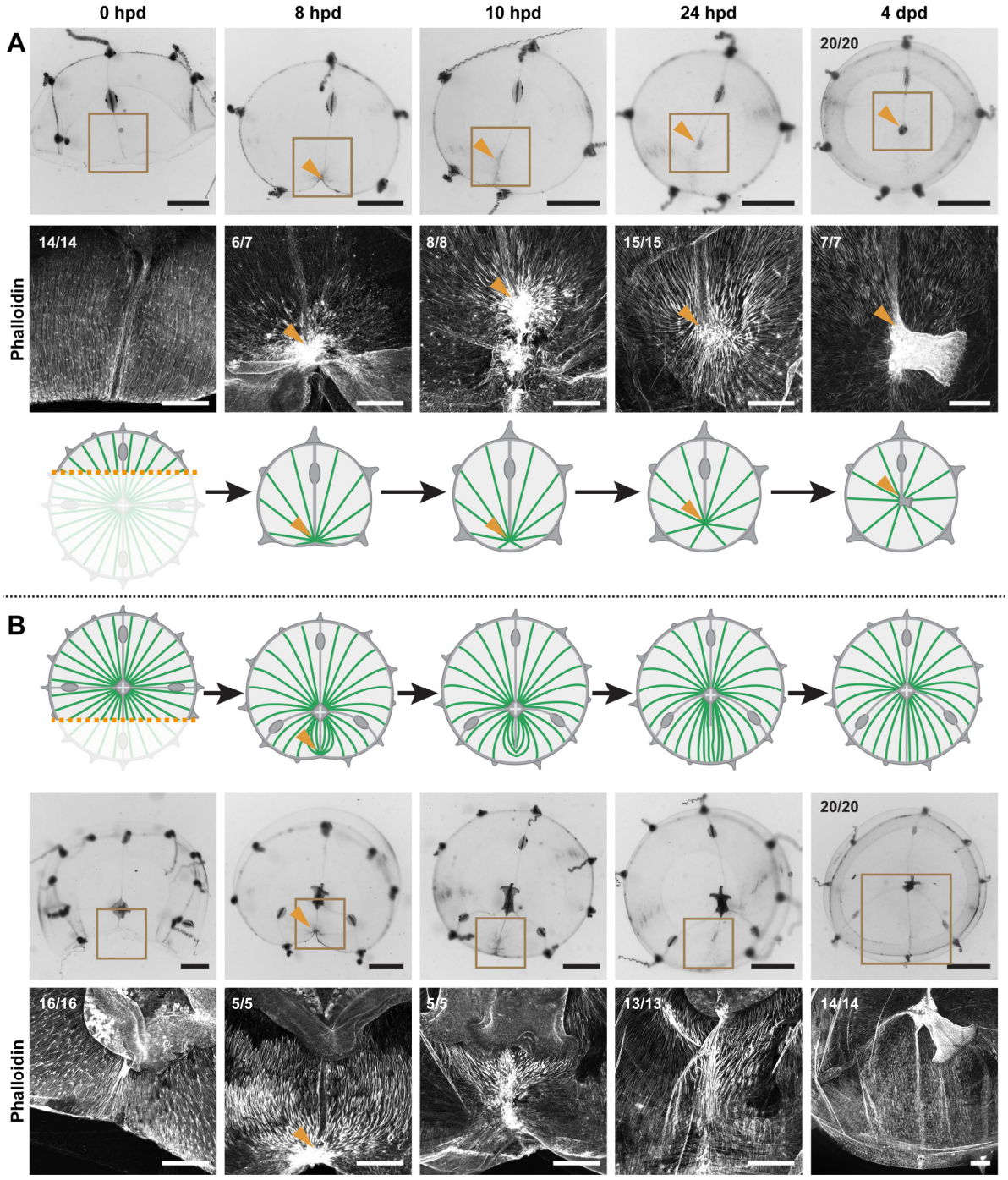


**Figure 9 – Hub stabilization is required for manubrium blastema formation.** (**A,B**) Behavior of radial muscle fibers in two medusa fragments generated from a bisection orthogonal to a radial canal, generating one smaller fragment without manubrium **(A)** and one larger fragment containing a manubrium **(B)**. Schematic comparison of the behavior of radial muscle fibers (green) in the two fragments at 0, 8, 10, 24 hpd and 4 dpd.

## Discussion

The topology of hydrozoan jellyfish, with a short primary body axis (oral/aboral), tetraradial body symmetry and pools of stem cells segregated into organs, offers a novel paradigm for studying the regulation of regenerative processes and of body patterning. We report here that swimming *Clytia* jellyfish cope efficiently with a wide range of damage, rapidly regaining functionality and a stable body organization. Such potential relies on robust mechanically-driven remodeling, which repositions organs and canals system and generates a novel transient structural landmark, a "hub" of reorganizing smooth muscle fibers, which predicts the site of manubrium blastema formation.

### Distinct contributions of tissue remodeling and cell proliferation to medusa regeneration

The relative contributions of cell proliferation (epimorphosis) and tissue remodeling (morphallaxis) to the restoration of forms and size have been long debated (Morgan, 1901). Research has largely focused on the dynamics of cell proliferation, while the contribution of remodeling has been understudied (Pellettieri, 2019). These processes often occur together, raising the question of their co-regulation. For instance in planarians, re-proportioning of body fragments is generally considered to follow blastema-based reformation of missing parts; when stem-cell based regeneration is prevented the expression of body pattern marker genes shifts nevertheless, indicating that re-patterning can occur independently of blastema formation (Gurley et al., 2010; Petersen and Reddien, 2009; Reddien et al., 2007). The balance between proliferation and remodeling during regeneration is quite variable among cnidarians: cell proliferation plays a prominent role in head regeneration in the polyps of *Nematostella* and *Hydractinia* (Amiel et al., 2015; Bradshaw et al., 2015; Passamaneck and Martindale, 2012) and in tentacle regeneration of some hydrozoan medusae (Fujita et al., 2019), while remodeling and repatterning of existing tissues are the main drivers of head regeneration in *Hydra* (Bode, 2003; Vogg et al., 2019).

Whole-body regeneration in *Clytia* jellyfish relies on both tissue remodeling and cell proliferation, whose contributions are coordinated, but spatially and temporally distinct. During an initial morphallactic phase, remodeling drives shape restoration, generating a novel spatial framework of structural elements. The subsequent epimorphic organ regeneration relies on cell proliferation. The heterogeneous cell mass from which the new manubrium regenerates can be regarded as a true blastema (Seifert and Muneoka, 2018). Its growth and morphogenesis into a functional organ involves extensive cell proliferation, but also targeted migration of *CheNanos1*-expressing cells, and the non-directed migration of a newly identified type of differentiated digestive cells, the MGD (Mobilizing

Gastro-Digestive) cells. The migration of putative stem cells towards the manubrium regeneration site is reminiscent of i-cell migration to the head blastema reported for *Hydractinia* polyps (Bradshaw et al., 2015) or the targeted migration of progenitors during planarian eye regeneration (Atabay et al., 2018). MGD cells represent an uncharacterized endodermal cell type whose mobilization via the canal system may be involved in regulating metabolic balance between organs.

**Wound healing and remodeling mechanically redefine jellyfish topology**

Following injury, an actomyosin cable rapidly assembles at the edge and contracts to progressively reduce the wound margin. Supracellular actomyosin cables generated by alignment of cortical actomyosin are a widespread feature of animal tissues, and are considered to be a conserved mechanism for the closure of epithelial gaps (Jain et al., 2019) in multiple contexts, including wound healing and morphogenesis (reviewed in (Röper, 2013; Schwayer et al., 2016). Actomyosin-based contractions have recently been documented during wound healing in *Clytia* exumbrella (Kamran et al., 2017), a simple tissue layer devoid of muscle fibers. For large umbrella injuries, the actomyosin-based wound-healing process is predicted to generate major tissue stresses, likely resisted by the stiffness of the mesoglea layer and of the umbrella margin, which condition the reorganization and final configuration of subumbrella elements.

Morphological “quadrants”, defined by a radial canal connecting a quarter manubrium, a gonad and tentacle bulb(s), repeat around the radial axis of the jellyfish. If none of the structural elements within a quadrant remains in a jellyfish fragment, quadrant self-organization cannot be triggered, and the entire morphological unit is lost. Thus, the angular position of elements ***around*** the radial axis is not encoded by a system of rotational coordinates, implying that the characteristic symmetry of the adult jellyfish does not depend on an actively maintained global patterning system. Conversely, self-organization efficiently restores any missing element in a quadrant ***along*** the radial axis. The nature of the patterning system acting operating along this axis remains to be elucidated.

How positional information is restored in animals undergoing regeneration remains a central question. Positional memory in amputated amphibian limbs is retained by connective cells, which instruct the pattern of the proliferating blastema (McCusker and Gardiner, 2013).Wound sites appears to act widely as signaling centers for the initiation of regeneration among animals (Owlarn et al., 2017), and in multiple instances have been shown to instruct the repatterning of body parts, such in *Hydra* polyps (Chera et al., 2009) or in zebrafish caudal fin (Wang et al., 2019). Planarian head blastemas also rely on the instructive role of the wound site (Oderberg et al., 2017; Petersen and Reddien, 2009; Reddien

and Alvarado, 2004; Wurtzel et al., 2015), which affect the expression of "Positional Control Genes" (PCGs) expressed along the longitudinal smooth muscles (Cebrià, 2016; Cutie et al., 2017; Reddien, 2018). In *Clytia* jellyfish, our tracing experiments show that the wound site correlates with the position where the blastema will form, however, not all wound sites will induce a blastema. Furthermore, blastema formation can be temporally uncoupled from wound healing, since it can be triggered several days later. Thus in *Clytia*, cues from the wound site do not directly or solely define the position of the feeding organ.

**A muscle-derived structural landmark for pattern formation**

During umbrella remodeling, severed radial smooth muscle fibers are pulled together by the wound healing process, leading to the emergence of a novel structural element, which we term the “hub". Stabilization of the hub transforms it into a landmark specifying the site of manubrium regeneration. We define this patterning system “spoke and hub”, where the presence of multiple muscle fiber “spokes” (vectors) converging at a hub determines the organ regeneration site.

The mechanisms regulating the stabilization, and final positioning of the muscle hub remain unclear. The "double hub" and “S/L dissection” experiments indicate that the topology of intact smooth muscle fiber "spokes" meeting at a hub is a reliable predictor of its fate: if the spokes are also connected to an existing hub, the new one will disassemble. While the initial catering of spokes is a consequence of the would-healing contraction process, the reorganization of muscle fibers into a “spoke and hub” configuration and the final positioning of the hub might be guided by mechanical tensions generated by the intact muscles anchored to the umbrella margin, reminiscent of *Drosophila* flight muscle assembly (Weitkunat et al., 2014). The alignment of myofibrils might also follow cell polarity cues, likely under the local control of the PCP signaling pathway (Seifert and Mlodzik, 2007), previously shown to orient epithelial cells during *Clytia* larval development (Momose et al., 2012).

Once the hub is stabilized and positioned, how does it trigger the manubrium blastema? One possibility involves a centro-peripheral gradient of morphogens, analogous to the positional signals encoded in planarian body muscles (Cebrià, 2016; Cutie et al., 2017; Reddien, 2018). Under this hypothesis, the confrontation of disparate positional values encoded in the myofibrils would trigger blastema formation. It is unclear, however, how such a system could achieve precision in the circular *Clytia* medusa. Alternatively the "spoke and hub" configuration could convert mechanical/cell polarity cues into biochemical signals, allowing the blastema site to be precisely defined within a broadly perturbed system.

There are now many examples of mechanical forces triggering biochemical responses (Chiou and Collins, 2018; Green and Sharpe, 2015; Ingber, 2003; Urdy, 2012; Vining and Mooney, 2017). Such integration can coordinate developmental processes (e.g. (Heisenberg and Bellaïche, 2013)), in particular promoting the accurate positioning of structures within a biological system. Long-range patterning is arduous to explain by biochemical signals alone (e.g. see (Das et al., 2019)), unless complex interactions are invoked to achieve precision (Oderberg et al., 2017). Regenerating *Hydra* polyps, a classic model for the study and conceptualization of morphogen gradient-based patterning (e.g. (Bode, 2009; Gierer and Meinhardt, 1972)), have been recently shown to rely on the alignment of supra-cellular actomyosin fibers for the determination of axis in regenerating fragments (Livshits et al., 2017; Mercker et al., 2015). In *Hydra*, it remains unclear how these mechanical cues are integrated with the well-known Wnt/β-catenin signaling, which patterns the primary body axis during both homeostasis and regeneration (Hobmayer et al., 2000; Nakamura et al., 2011).

In *Clytia* jellyfish the hub center likely represents a site of low muscle tension, which could via induction of an undetermined signaling system trigger blastema formation. An alternative hypothesis is that the spokes carry intrinsic polarity, and that when opposing PCP vectors meet at the hub this confrontation triggers blastema formation.

"Spoke and hub" muscle configurations equivalent to the one we describe here in *Clytia* can be recognized during wound healing/regeneration in both *Hydra* (Livshits et al., 2017) and planarians (Scimone et al., 2017), preceding the appearance of a new mouth or blastema. "Spoke and hub" patterning systems might thus represent a general but overlooked feature of regenerating animals, playing an early role in the stabilization of remodeling tissues and in the precise positioning of new structures.

## Materials and methods

### *Clytia hemisphaerica* husbandry

*Clytia* jellyfish were clonally grown from Z4B (female) polyp colony (see (Leclère et al., 2019)) for further information on the genome and the establishment of the line), in the *Clytia* facility at IMEV, according to the method developed by (Lechable et al., 2019) (custom-made closed system, in artificial sea water at 18°C, fed twice a day with *Artemia sp*. nauplii). We performed all experiments on 11-14 days old individuals (diameter 0.5 – 0.8 cm), corresponding to newly matured medusae (spawning). Selected animals were not fed for at least 12 hours prior to experiments; and generally not fed during regeneration experiments, with the exception of some of the gonad and bulb-regeneration experiments and of the fluorescent bead assay (see later).

### Surgical procedures

Surgical manipulations were performed on agarose-coated petri dishes (2% agarose in filtered artificial sea water or FASW), by means of custom-made tools made of fine platinum wire, acupuncture needles, pipette tips of diverse diameters, Dowell scissors (Fine Science Tools #15040-11), fine forceps (Fine Science Tools #11370-40) and fine scalpels. For manipulations, animals were relaxed either with ice-cold FASW or menthol in FASW (400 µM). Tentacles were trimmed with fine scissors, to avoid damages to the animals due to entangling. Operated animals were kept in a clean multi-well plate, in 5 ml of FASW with antibiotics (penicillin plus streptomycin), which was refreshed at least once per day; multi-well plates were kept in an incubator, at 18°C, agitating.
Organ dissections were performed either by punching out the corresponding area in the umbrella using an appropriately-sized pipette tip (thus generating a hole across subumbrella, mesoglea and exumbrella), or by excising the targeted element by means of forceps and a scalpel or with custom-made wire tools (minimizing umbrella damage). Grafts were performed by means of acupuncture needles, used to stich fragments together, and fine forceps.
Experiments were monitored at least once per day, and pictures were taken when necessary (see later). For imaging, animals were temporarily relaxed with menthol in FASW (400 µM).

### *In-vivo* cell labeling experiments

EdU labeling was performed by incubating medusae in a 100 µM solution (EdU in FASW; EdU from Thermofisher Click-It kit, #C10338), for the designed amount of time (pulse and pulse-chase experiments; incubation times are reported in the Results section). Animals were then fixed with 4% paraformaldehyde (PFA) in 1X PBS, for two hours, then rinsed with 1x PBS. Staining was performed with the EdU Click-It kit (Alexa Fluor 555 kit; ThermoFisher #C10338), following the manufacturer

protocol (BSA not added). Nuclei were counterstained with 1 µg/ml Hoechst 33258 (Sigma-Aldrich #94403). Fluorescent beads labeling (FluoSpheres, Molecular Probes #F8812) was performed by feeding animals with beads mixed to hatched artemia. Beads were first washed through five successive centrifugations in mQ $H_2O$ and resuspended in mQ $H_2O$. Artemia nauplii were then incubated with the beads for one hour. After feeding, jellyfish were washed with FASW, to remove the non-ingested beads.

**Chemical treatments**

Cell proliferation was blocked by treating animals with 10 mM hydroxyurea (Sigma-Aldrich #H8627) dissolved in FASW; the solution was renewed twice a day. Muscle contraction was inhibited by means of: 34 mM blebbistatin (Sigma-Aldrich #B0560) dissolved in DMSO, 8 mM BDM (2,3-Butanedione monoxime; Sigma-Aldrich #B0753) in FASW, 400 µM menthol (Sigma-Aldrich #M2772) in ethanol (1M stock solution).

**In situ hybridization, immunostaining and phalloidin staining**

Fluorescent in situ hybridization and probe synthesis were performed according to the urea-based protocol developed in ((Sinigaglia et al., 2018), see also (Sinigaglia, 2019) for recipes and reagents). For immunostaining, animals were fixed for two hours with 4% PFA in HEPES buffer (HEPES 0,1M, EGTA 50mM, MgSO4 10mM, Maltose 80mM), rinsed and permeabilized with 1X PBS plus Triton X-100 (0.2%), blocked and incubated with the anti-pMyo antibody (1:200, rabbit; Cell signaling technology #3671), or the anti-tyrosinated tubulin antibody YL1/2 (1:50, rat; Abcam #6160), detected with a goat anti-rabbit secondary antibody coupled to rhodamine (1:500) and a goat anti-rat secondary antibody coupled to Alexa 594 (1:200; Thermo-Fisher #A-11006 and #A-11007), and mounted in Citifluor AF-1 (Citifluor #AF1-100) for imaging. Actin fibers were stained with 1:100 phalloidin coupled to Alexa 488 (solubilized in methanol and dried prior to use; Fisher Scientific #10125092), following fixation with 4% formaldehyde in HEPES buffer. For FISH plus EdU reaction, animals were fixed with 3,7% formaldehyde in HEPES buffer and the EdU click-It reaction was performed after the TSA reaction of FISH. Nuclei were counterstained with 1 µg/ml Hoechst 33258 (Sigma-Aldrich #94403).

**Image acquisition and processing**

Macroscopic images were taken with a Sony camera (NEX-5R), mounted on an Olympus SZ61 stereoscope. Fluorescent images were taken with a Zeiss Axio Imager A2 microscope and with a Leica SP8 confocal microscope. Image processing (maximum projection, color display), and

quantifications were done with the Fiji software. Plots were drawn with the ggplot package of R. Drawings and composition of figures were done with Illustrator CS6 (Adobe).

### Statistics

Statistical testing was performed with R. Specific tests employed are reported in the figure legends.

## Acknowledgements

We thank Josselin Lupette, Sophie Rei-Rosa, Priscilla Freschu, Gwladys Perez, Emma Labis and Sandra Chevalier for technical assistance, and Sophie Collet, Loann Gissat, Alexandre Jan and Laurent Gilletta for animal maintenance. We further thank Yulia Kraus for grafting advice, Severine Urdy for discussions, and Michalis Averof for comments on the manuscript. This work was supported by a grant from the Agence Nationale de la Recherche (#ANR-13-PDOC-0016), core CNRS and Sorbonne University funding to the LBDV; PhD fellowships for SP from the Ministère de l'Enseignement Supérieur et de la Recherche and the Fondation pour la Recherche Médicale (#FDT201805005536). We thank the Marine Resources Centre (CRBM and PIV imaging platform) of Institut de la Mer de Villefranche (IMEV) that is supported by EMBRC-France, whose French state funds are managed by the ANR within the investments of the Future program (#ANR-10-INBS-02).

## References

Abrams MJ, Basinger T, Yuan W, Guo C-L, Goentoro L. 2015. Self-repairing symmetry in jellyfish through mechanically driven reorganization. *Proc Natl Acad Sci U S A* **112**:E3365-3373. doi:10.1073/pnas.1502497112

Amiel AR, Johnston HT, Nedoncelle K, Warner JF, Ferreira S, Röttinger E. 2015. Characterization of Morphological and Cellular Events Underlying Oral Regeneration in the Sea Anemone, Nematostella vectensis. *Int J Mol Sci* **16**:28449–28471. doi:10.3390/ijms161226100

Atabay KD, LoCascio SA, de Hoog T, Reddien PW. 2018. Self-organization and progenitor targeting generate stable patterns in planarian regeneration. *Science* **360**:404–409.

Begnaud S, Chen T, Delacour D, Mège R-M, Ladoux B. 2016. Mechanics of epithelial tissues during gap closure. *Curr Opin Cell Biol* **42**:52–62. doi:10.1016/j.ceb.2016.04.006

Bode H. 2011. Axis formation in hydra. *Annu Rev Genet* **45**:105–117. doi:10.1146/annurev-genet-102209-163540

Bode HR. 2009. Axial patterning in hydra. *Cold Spring Harb Perspect Biol* **1**:a000463. doi:10.1101/cshperspect.a000463

Bode HR. 2003. Head regeneration in Hydra. *Dev Dyn Off Publ Am Assoc Anat* **226**:225–236. doi:10.1002/dvdy.10225

Bosch TCG. 2009. Hydra and the evolution of stem cells. *BioEssays News Rev Mol Cell Dev Biol* **31**:478–486. doi:10.1002/bies.200800183

Bradshaw B, Thompson K, Frank U. 2015. Distinct mechanisms underlie oral vs aboral regeneration in the cnidarian Hydractinia echinata. *eLife* **4**:e05506. doi:10.7554/eLife.05506

Cebrià F. 2016. Planarian Body-Wall Muscle: Regeneration and Function beyond a Simple Skeletal Support. *Front Cell Dev Biol* **4**:8. doi:10.3389/fcell.2016.00008

Chera S, Ghila L, Dobretz K, Wenger Y, Bauer C, Buzgariu W, Martinou J-C, Galliot B. 2009. Apoptotic cells provide an unexpected source of Wnt3 signaling to drive hydra head regeneration. *Dev Cell* **17**:279–289. doi:10.1016/j.devcel.2009.07.014

Chiou K, Collins E-MS. 2018. Why we need mechanics to understand animal regeneration. *Dev Biol* **433**:155–165. doi:10.1016/j.ydbio.2017.09.021

Cutie S, Hoang AT, Payumo AY, Huang GN. 2017. Unconventional Functions of Muscles in Planarian Regeneration. *Dev Cell* **43**:657–658. doi:10.1016/j.devcel.2017.12.006

Das D, Jülich D, Schwendinger-Schreck J, Guillon E, Lawton AK, Dray N, Emonet T, O'Hern CS, Shattuck MD, Holley SA. 2019. Organization of Embryonic Morphogenesis via Mechanical Information. *Dev Cell* **49**:829-839.e5. doi:10.1016/j.devcel.2019.05.014

Denker E, Manuel M, Leclère L, Le Guyader H, Rabet N. 2008. Ordered progression of nematogenesis from stem cells through differentiation stages in the tentacle bulb of Clytia hemisphaerica (Hydrozoa, Cnidaria). *Dev Biol* **315**:99–113. doi:10.1016/j.ydbio.2007.12.023

DuBuc TQ, Dattoli AA, Babonis LS, Salinas-Saavedra M, Röttinger E, Martindale MQ, Postma M. 2014. In vivo imaging of Nematostella vectensis embryogenesis and late development using fluorescent probes. *BMC Cell Biol* **15**:44. doi:10.1186/s12860-014-0044-2

French V, Bryant PJ, Bryant SV. 1976. Pattern Regulation in Epimorphic Fields. *Science* **193**:969–981.

Fujita S, Kuranaga E, Nakajima Y-I. 2019. Cell proliferation controls body size growth, tentacle morphogenesis, and regeneration in hydrozoan jellyfish Cladonema pacificum. *PeerJ* **7**:e7579. doi:10.7717/peerj.7579

Gahan JM, Bradshaw B, Flici H, Frank U. 2016. The interstitial stem cells in Hydractinia and their role in regeneration. *Curr Opin Genet Dev* **40**:65–73. doi:10.1016/j.gde.2016.06.006

Galliot B. 2012. Hydra, a fruitful model system for 270 years. *Int J Dev Biol* **56**:411–423. doi:10.1387/ijdb.120086bg

Gierer A, Meinhardt H. 1972. A theory of biological pattern formation. *Kybernetik* **12**:30–39. doi:10.1007/bf00289234

Green JBA, Sharpe J. 2015. Positional information and reaction-diffusion: two big ideas in developmental biology combine. *Dev Camb Engl* **142**:1203–1211. doi:10.1242/dev.114991

Gurley KA, Elliott SA, Simakov O, Schmidt HA, Holstein TW, Sánchez Alvarado A. 2010. Expression of secreted Wnt pathway components reveals unexpected complexity of the planarian amputation response. *Dev Biol* **347**:24–39. doi:10.1016/j.ydbio.2010.08.007

Hargitt CW. 1899. Experimental studies upon Hydromedusae. *Biol Bull* **1**:35–51.

Hargitt GT. 1903. Regeneration in hydromedusae. *Dev Genes Evol* **17**:64–91.

Heisenberg C-P, Bellaïche Y. 2013. Forces in tissue morphogenesis and patterning. *Cell* **153**:948–962. doi:10.1016/j.cell.2013.05.008

Hobmayer B, Rentzsch F, Kuhn K, Happel CM, von Laue CC, Snyder P, Rothbächer U, Holstein TW. 2000. WNT signalling molecules act in axis formation in the diploblastic metazoan Hydra. *Nature* **407**:186–189. doi:10.1038/35025063

Houliston E, Momose T, Manuel M. 2010. Clytia hemisphaerica: a jellyfish cousin joins the laboratory. *Trends Genet TIG* **26**:159–167. doi:10.1016/j.tig.2010.01.008

Ingber DE. 2003. Mechanobiology and diseases of mechanotransduction. *Ann Med* **35**:564–577. doi:10.1080/07853890310016333

Jain A, Ulman V, Mukherjee A, Prakash M, Pimpale L, Muenster S, Panfilio KA, Jug F, Grill SW, Tomancak P, Pavlopoulos A. 2019. Regionalized tissue fluidization by an actomyosin cable is required for epithelial gap closure during insect gastrulation. *bioRxiv* 744193. doi:10.1101/744193

Kamran Z, Zellner K, Kyriazes H, Kraus CM, Reynier J-B, Malamy JE. 2017. In vivo imaging of epithelial wound healing in the cnidarian Clytia hemisphaerica demonstrates early evolution of purse string and cell crawling closure mechanisms. *BMC Dev Biol* **17**:17. doi:10.1186/s12861-017-0160-2

Lander AD. 2013. How cells know where they are. *Science* **339**:923–927. doi:10.1126/science.1224186

Lechable M, Jan A, Weissbourd B, Uveira J, Gissat L, Collet S, Gilletta L, Chevalier S, Leclère L, Peron S, Barreau C, Lasbleiz R, Houliston E, Momose T. 2019. An improved whole life cycle culture protocol for the hydrozoan genetic model Clytia hemisphaerica. *bioRxiv* 852632. doi:10.1101/852632

Leclère L, Copley RR, Momose T, Houliston E. 2016. Hydrozoan insights in animal development and evolution. *Curr Opin Genet Dev* **39**:157–167. doi:10.1016/j.gde.2016.07.006

Leclère L, Horin C, Chevalier S, Lapébie P, Dru P, Peron S, Jager M, Condamine T, Pottin K, Romano S, Steger J, Sinigaglia C, Barreau C, Quiroga Artigas G, Ruggiero A, Fourrage C, Kraus JEM, Poulain J, Aury J-M, Wincker P, Quéinnec E, Technau U, Manuel M, Momose T, Houliston E, Copley RR. 2019. The genome of the jellyfish Clytia hemisphaerica and the evolution of the cnidarian life-cycle. *Nat Ecol Evol* **3**:801–810. doi:10.1038/s41559-019-0833-2

Leclère L, Jager M, Barreau C, Chang P, Le Guyader H, Manuel M, Houliston E. 2012. Maternally localized germ plasm mRNAs and germ cell/stem cell formation in the cnidarian Clytia. *Dev Biol* **364**:236–248. doi:10.1016/j.ydbio.2012.01.018

Leclère L, Röttinger E. 2016. Diversity of Cnidarian Muscles: Function, Anatomy, Development and Regeneration. *Front Cell Dev Biol* **4**:157. doi:10.3389/fcell.2016.00157

Livshits A, Shani-Zerbib L, Maroudas-Sacks Y, Braun E, Keren K. 2017. Structural Inheritance of the Actin Cytoskeletal Organization Determines the Body Axis in Regenerating Hydra. *Cell Rep* **18**:1410–1421. doi:10.1016/j.celrep.2017.01.036

McCusker CD, Gardiner DM. 2013. Positional information is reprogrammed in blastema cells of the regenerating limb of the axolotl (Ambystoma mexicanum). *PloS One* **8**:e77064. doi:10.1371/journal.pone.0077064

Meinhardt H. 1993. A model for pattern formation of hypostome, tentacles, and foot in hydra: how to form structures close to each other, how to form them at a distance. *Dev Biol* **157**:321–333. doi:10.1006/dbio.1993.1138

Mercker M, Köthe A, Marciniak-Czochra A. 2015. Mechanochemical symmetry breaking in hydra aggregates. *Biophys J* **108**:2396–2407.

Momose T, De Cian A, Shiba K, Inaba K, Giovannangeli C, Concordet J-P. 2018. High doses of CRISPR/Cas9 ribonucleoprotein efficiently induce gene knockout with low mosaicism in the hydrozoan Clytia hemisphaerica through microhomology-mediated deletion. *Sci Rep* **8**:11734. doi:10.1038/s41598-018-30188-0

Momose T, Kraus Y, Houliston E. 2012. A conserved function for Strabismus in establishing planar cell polarity in the ciliated ectoderm during cnidarian larval development. *Dev Camb Engl* **139**:4374–4382. doi:10.1242/dev.084251

Morgan TH. 1901. Regeneration. Cambridge University Press. doi:10.1017/CBO9781107415324.004

Morgan TH. 1899. Regeneration in the Hydromedusa, Gonionemus vertens. *Am Nat* **33**:939–951.

Nakamura Y, Tsiairis CD, Özbek S, Holstein TW. 2011. Autoregulatory and repressive inputs localize Hydra Wnt3 to the head organizer. *Proc Natl Acad Sci U S A* **108**:9137–9142. doi:10.1073/pnas.1018109108

Neppi V. 1918. Sulla rigenerazione nelle idromeduse. *Pubblicazioni Della Stazione Zool Napoli* **2**:191–207.

Oderberg IM, Li DJ, Scimone ML, Gaviño MA, Reddien PW. 2017. Landmarks in existing tissue at wounds are utilized to generate pattern in regenerating tissue. *Curr Biol* **27**:733–742.

Owlarn S, Klenner F, Schmidt D, Rabert F, Tomasso A, Reuter H, Mulaw MA, Moritz S, Gentile L, Weidinger G, Bartscherer K. 2017. Generic wound signals initiate regeneration in missing-tissue contexts. *Nat Commun* **8**:2282. doi:10.1038/s41467-017-02338-x

Passamaneck YJ, Martindale MQ. 2012. Cell proliferation is necessary for the regeneration of oral structures in the anthozoan cnidarian Nematostella vectensis. *BMC Dev Biol* **12**:34. doi:10.1186/1471-213X-12-34

Pellettieri J. 2019. Regenerative tissue remodeling in planarians - The mysteries of morphallaxis. *Semin Cell Dev Biol* **87**:13–21. doi:10.1016/j.semcdb.2018.04.004

Petersen CP, Reddien PW. 2009. A wound-induced Wnt expression program controls planarian regeneration polarity. *Proc Natl Acad Sci* **106**:17061–17066.

Raz AA, Srivastava M, Salvamoser R, Reddien PW. 2017. Acoel regeneration mechanisms indicate an ancient role for muscle in regenerative patterning. *Nat Commun* **8**:1260. doi:10.1038/s41467-017-01148-5

Reddien PW. 2018. The cellular and molecular basis for planarian regeneration. *Cell* **175**:327–345.

Reddien PW, Alvarado AS. 2004. Fundamentals of planarian regeneration. *Annu Rev Cell Dev Biol* **20**:725–757.

Reddien PW, Bermange AL, Kicza AM, Alvarado AS. 2007. BMP signaling regulates the dorsal planarian midline and is needed for asymmetric regeneration. *Development* **134**:4043–4051.

Röper K. 2013. Supracellular actomyosin assemblies during development. *Bioarchitecture* **3**:45–49. doi:10.4161/bioa.25339

Schaffer AA, Bazarsky M, Levy K, Chalifa-Caspi V, Gat U. 2016. A transcriptional time-course analysis of oral vs. aboral whole-body regeneration in the Sea anemone Nematostella vectensis. *BMC Genomics* **17**:718. doi:10.1186/s12864-016-3027-1

Schmid V. 1974. Regeneration in medusa buds and medusae of Hydrozoa. *Am Zool* **14**:773–781.

Schmid V, Alder H. 1984. Isolated, mononucleated, striated muscle can undergo pluripotent transdifferentiation and form a complex regenerate. *Cell* **38**:801–809.

Schmid V, Schmid B, Schneider B, Stidwill R, Baker G. 1976. Factors effecting manubrium-regeneration in hydromedusae (Coelenterata). *Dev Genes Evol* **179**:41–56.

Schmid V, Tardent P. 1971. The reconstitutional performances of the Leptomedusa Campanularia jonstoni. *Mar Biol* **8**:99–104.

Schwayer C, Sikora M, Slováková J, Kardos R, Heisenberg C-P. 2016. Actin Rings of Power. *Dev Cell* **37**:493–506. doi:10.1016/j.devcel.2016.05.024

Scimone ML, Cote LE, Reddien PW. 2017. Orthogonal muscle fibres have different instructive roles in planarian regeneration. *Nature* **551**:623–628. doi:10.1038/nature24660

Seifert AW, Muneoka K. 2018. The blastema and epimorphic regeneration in mammals. *Dev Biol* **433**:190–199. doi:10.1016/j.ydbio.2017.08.007

Seifert JRK, Mlodzik M. 2007. Frizzled/PCP signalling: a conserved mechanism regulating cell polarity and directed motility. *Nat Rev Genet* **8**:126–138. doi:10.1038/nrg2042

Sinigaglia C. 2019. A Widely Applicable Urea-based Fluorescent/Colorimetric mRNA in situ Hybridization Protocol. *Bio-Protoc* 9(17), e3360.

Sinigaglia C, Thiel D, Hejnol A, Houliston E, Leclère L. 2018. A safer, urea-based in situ hybridization method improves detection of gene expression in diverse animal species. *Dev Biol* **434**:15–23.

Urdy S. 2012. On the evolution of morphogenetic models: mechano-chemical interactions and an integrated view of cell differentiation, growth, pattern formation and morphogenesis. *Biol Rev* **87**:786–803.

Vining KH, Mooney DJ. 2017. Mechanical forces direct stem cell behaviour in development and regeneration. *Nat Rev Mol Cell Biol* **18**:728–742. doi:10.1038/nrm.2017.108

Vogg MC, Galliot B, Tsiairis CD. 2019. Model systems for regeneration: Hydra. *Dev Camb Engl* **146**. doi:10.1242/dev.177212

Wang Y-T, Tseng T-L, Kuo Y-C, Yu J-K, Su Y-H, Poss KD, Chen C-H. 2019. Genetic Reprogramming of Positional Memory in a Regenerating Appendage. *Curr Biol CB* **29**:4193-4207.e4. doi:10.1016/j.cub.2019.10.038

Weitkunat M, Kaya-Çopur A, Grill SW, Schnorrer F. 2014. Tension and force-resistant attachment are essential for myofibrillogenesis in Drosophila flight muscle. *Curr Biol* **24**:705–716.

Witchley JN, Mayer M, Wagner DE, Owen JH, Reddien PW. 2013. Muscle cells provide instructions for planarian regeneration. *Cell Rep* **4**:633–641. doi:10.1016/j.celrep.2013.07.022

Wurtzel O, Cote LE, Poirier A, Satija R, Regev A, Reddien PW. 2015. A Generic and Cell-Type-Specific Wound Response Precedes Regeneration in Planarians. *Dev Cell* **35**:632–645. doi:10.1016/j.devcel.2015.11.004

## Supplementary Figures

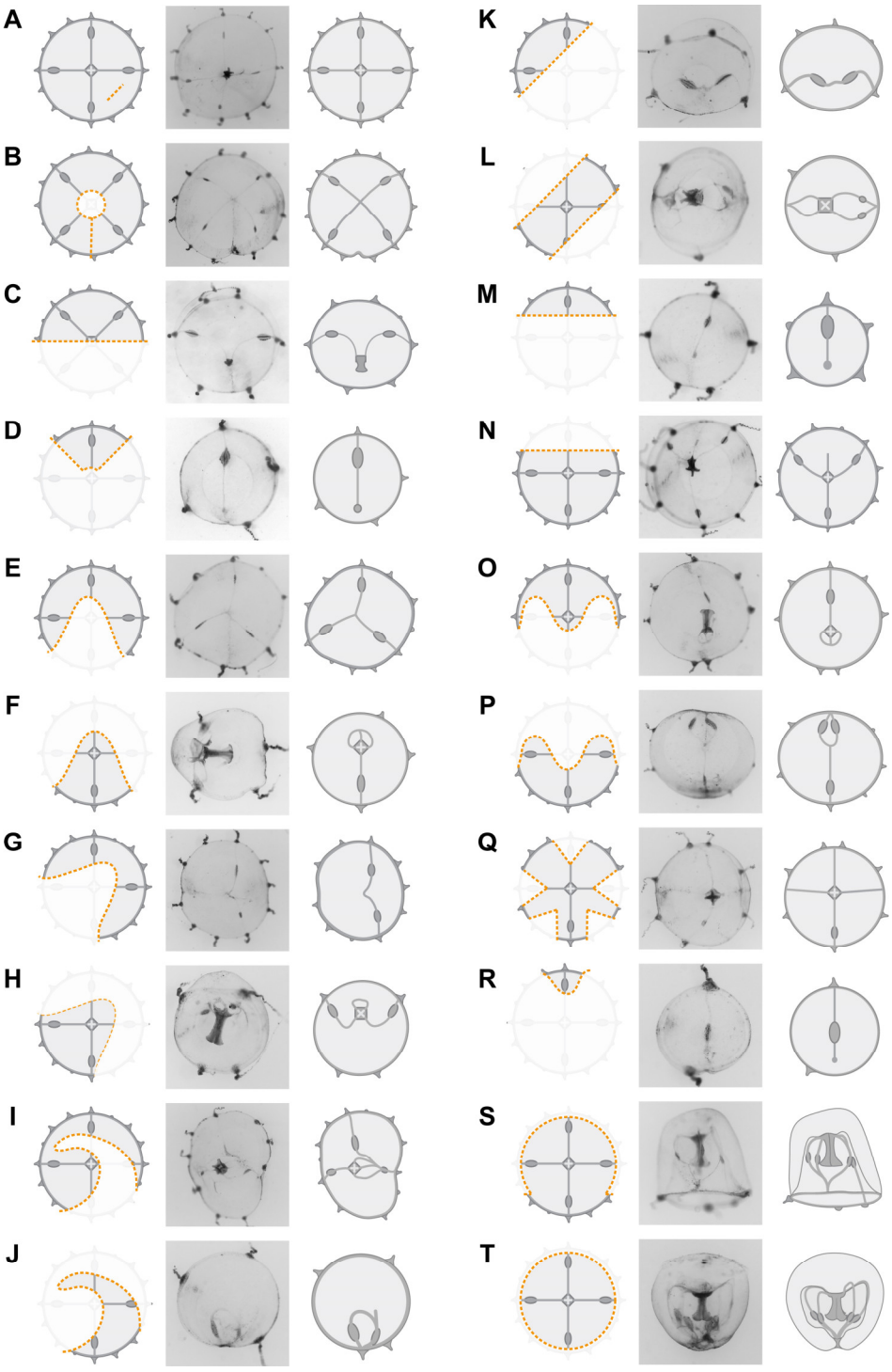


**Figure 1.S1 – Umbrella restorative potential.** Any type of damage **(A-T)** triggers the remodeling of the umbrella, driven by a rapid reduction of the cut edges. The segments of severed peripheral circular canal fuse together, and constrain the final perimeter of the animal. The circular shape is always restored, while the original tetraradial symmetry is usually not recovered (exceptions in A, B). Left: diagram of dissection (yellow dotted line, removed parts are masked); Right: picture and diagram of resulting medusa morphology, after 24 hpd. C, D and T show images displayed also in Figure 8A, 1I and 1J, respectively.

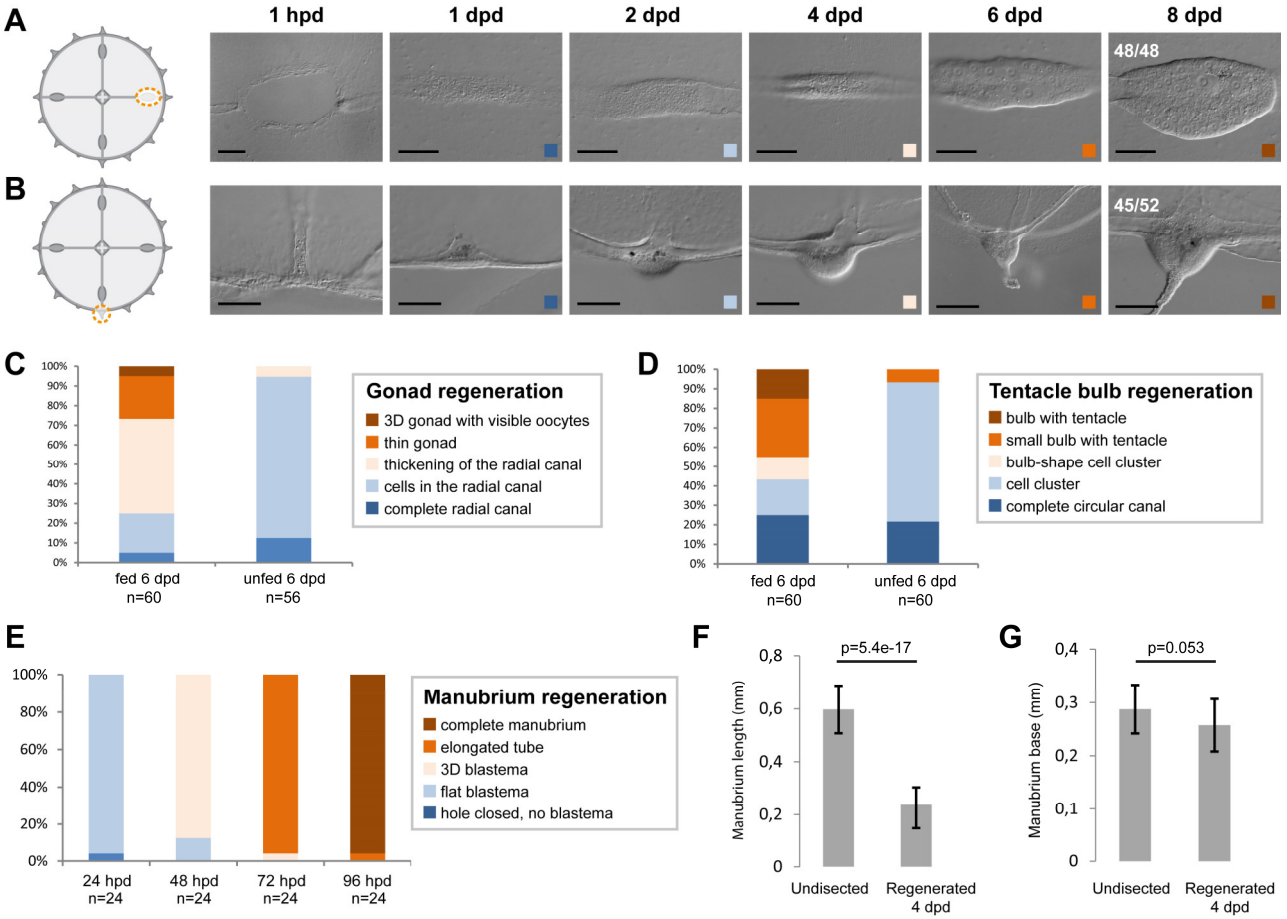


**Figure 1.S2 – Organ regeneration. (A-E)** Organ regeneration in relation to feeding status. **A)** Gonad and **B)** tentacle bulb regenerate in 6 days, in fed individuals. **C,D)** In the case of gonads and bulbs, regeneration rate is variable and depends on the feeding status of the medusa (gonads in **C**, tentacle bulbs in **D**), while **E)** manubrium regeneration is highly stereotypic. **(F)** Regenerated manubria are shorter than the endogenous ones (measured from base to lip, 20 jellyfish), **(G)** even if the base occupies a comparable size. Test: two tailed t-test. A and B show images also displayed in Figure 1F and 1G, respectively. Scale bars: 100 µm.

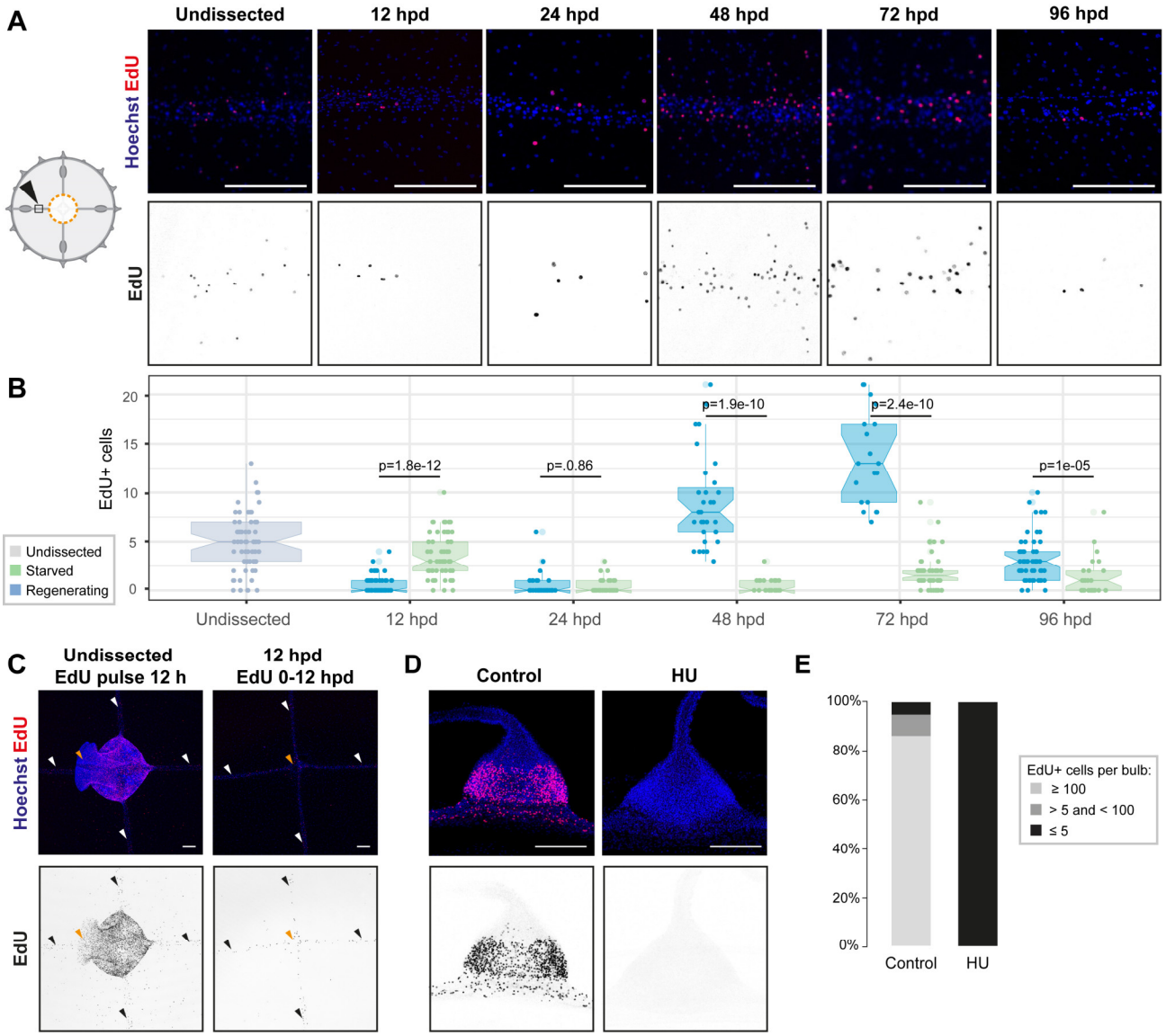


**Figure 2.S1 – Dynamics of cell proliferation during regeneration. (A, B)** Cycling cells can be detected in the MG-segment of radial canals (EdU pulse; quantified in **B**). Proliferation levels drop following manubrium ablation, then increase again between 48 hpd and 72 hpd. **B)** Increase of proliferation is specific to regenerating medusae, while starvation reduces the number of cycling cells. Statistical test: Mann Whitney Wilcoxon. **(C)** Proliferation levels during a 12 hours EdU pulse in regenerating vs non-regenerating medusae: no increase of cell proliferation is observed during the first 12 hours post-dissection. **(D, E)** HU-treatment successfully inhibits cell proliferation, as shown by the absence of EdU-positive cells in the tentacle bulb (quantification in **E**), a highly proliferating stem cell niche. Scale bars: 100µm.

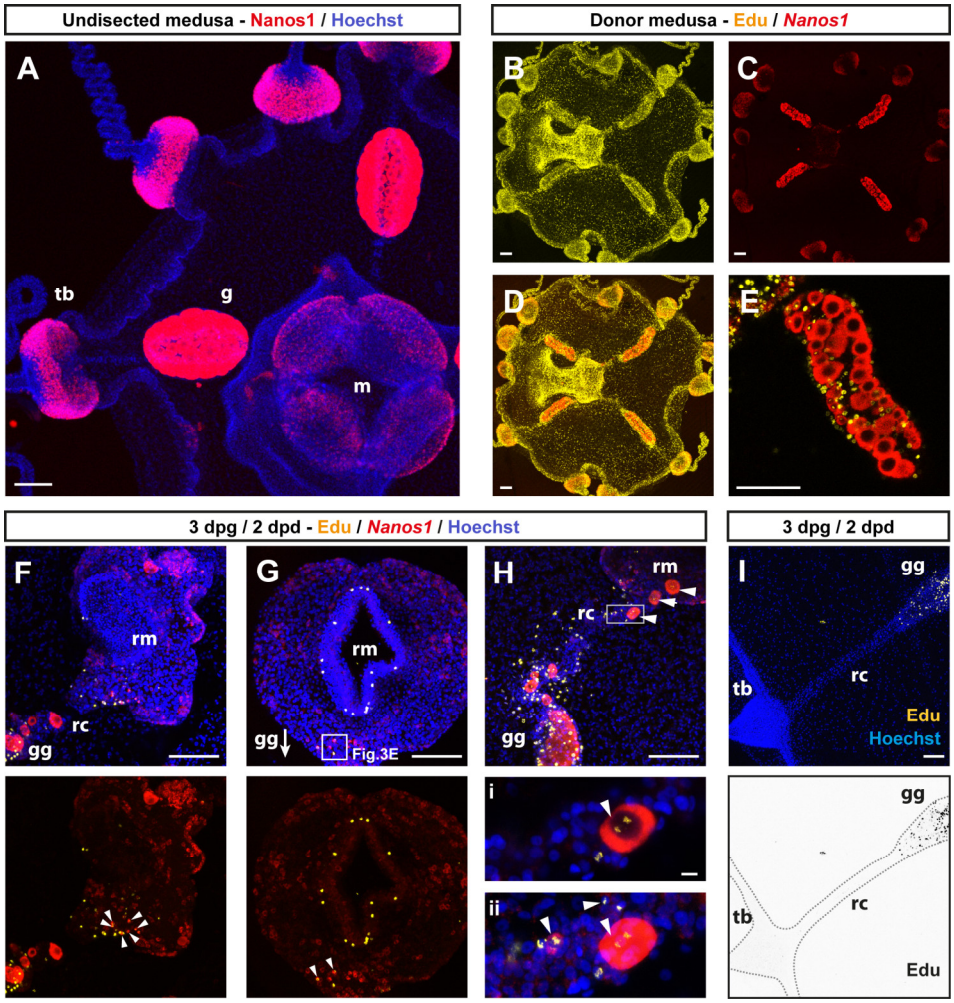


**Figure 3.S1 – Supplementary information related to Figure 3. (A)** Fluorescent in situ hybridization (FISH) showing the localization of *CheNanos1*-expressing cells (shown in magenta), in a two weeks old un-operated medusa. **(B-E)** Gonad-donor medusae, showing double staining for EdU (EdU only in **B**, yellow) and *CheNanos1* (FISH only in **C**, red), overlay in **D**. **E)** Gonad of a donor medusae, showing EdU+/*CheNanos1*+ cells in the gonad (single plane). **(F,G,H)** Three specimens of gonad-grafted regenerating medusae showing EdU+ cells (in yellow) as well as EdU+/Nanos1+ (*Nanos1*+ in red) cells in the regenerating manubrium and in the connecting canal. White square in G corresponds to the area shown in figure 3E. **H)** EdU/*Nanos1* double positive small oocytes (white arrowheads), originating from the grafted gonad, are found in the regenerating manubrium and within the connecting canal. The fate of those maturing germ cells remains to be investigated. Lower panel: close up (i, single plane; ii, maximum projection) corresponding to the square shown on the upper panel. **(I)** EdU-positive cells are not found in the tentacle bulb or the portion of the radial canal comprised between bulb and the EdU+ grafted gonad. Abbreviations: m: manubrium, rm: regenerating manubrium, g: gonad, gg: grafted gonad. tb: tentacle bulb, rc: radial canal. Scale bars: 100 µm, except in the lower panels of (H): 10 µm.

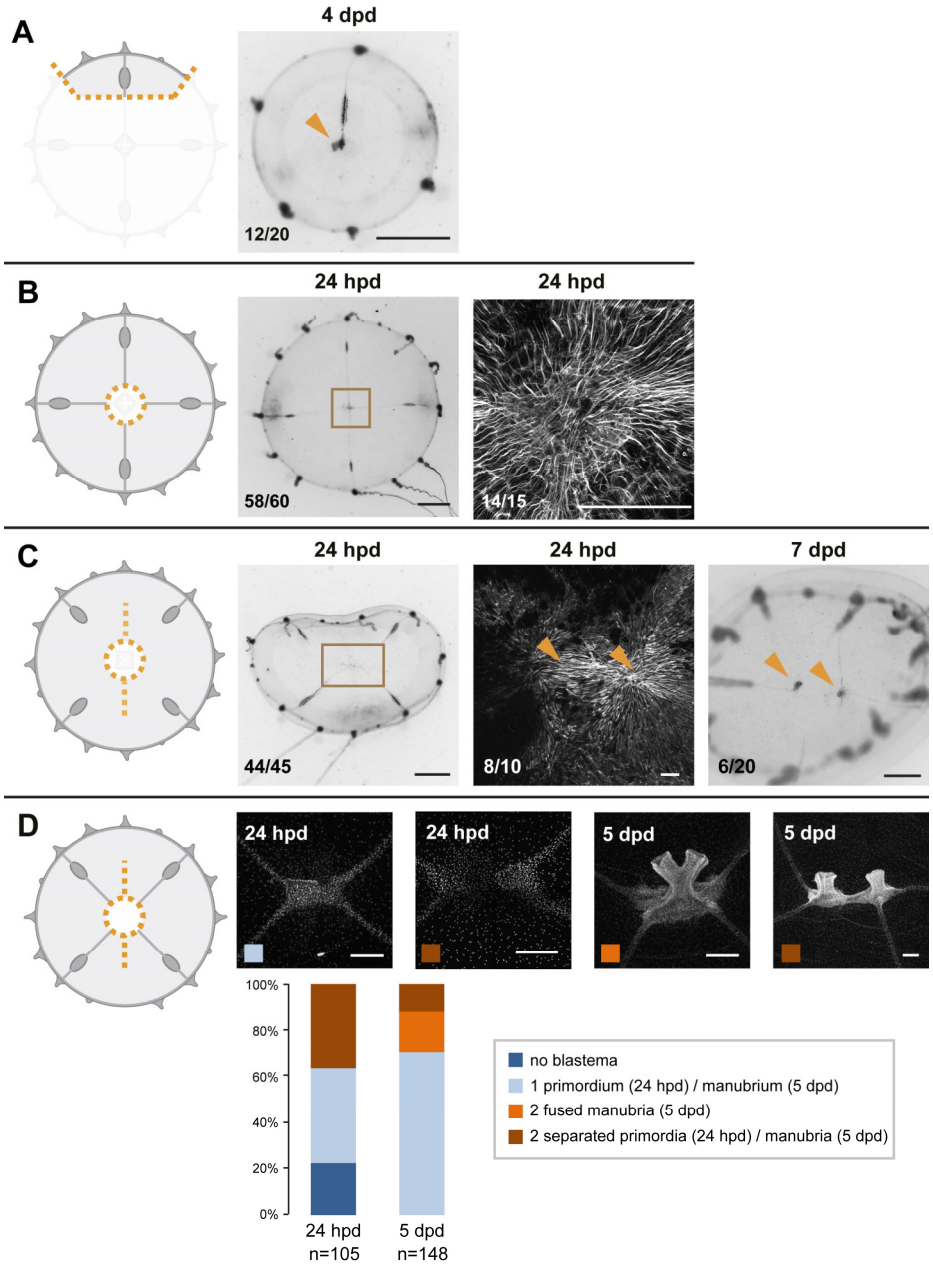


**Figure 6.S1 – Supplementary information related to Figure 6. (A)** Smaller fragments of the interradial quarter (left panel) also regenerate a manubrium (right panel), showing that the potential for manubrium regeneration is not restricted to the more central region of the umbrella. **(B)** Radial smooth muscle fibers join at the center of the medusa after manubrium ablation, forming a "muscle hub" systematically associated with primordium formation. Phalloidin staining of the muscle hub 24 hpd (right panel) is the same shown in figure 2A. **(C)** Radial canals are not necessary for the formation of muscle hubs. Phalloidin staining shows that a double hub forms also when the adjoining canal segments are removed, leading in some cases into the regeneration of two manubria, once at least one canal regrows to each hub. **(D)** The ablation of manubrium coupled to a longitudinal dissection of the umbrella can result in different outcomes, quantified at 24 hpd and 5 dpd: regenerating anlages might fuse, at blastema or later stages, or remain separated. Confocal images show Hoechst staining. Scale bars: 1mm for DIC medusae images, 200 µm for confocal images.

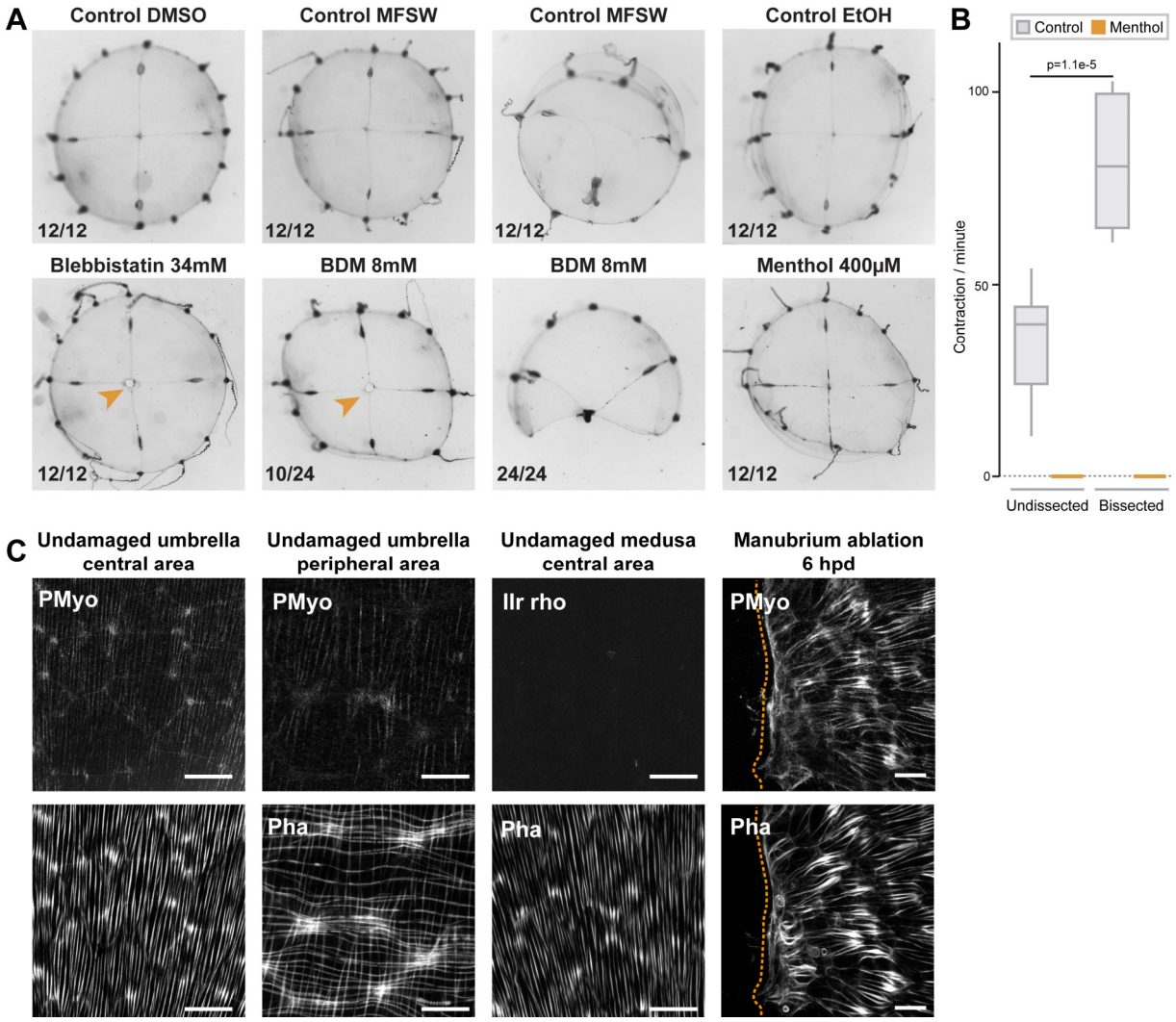


**Figure 8.S1** – **Actomyosin based remodeling. (A)** Myosin inhibitor (blebbistatin and BDM) treatments demonstrate that wound healing and remodeling depend on the action of actin-myosin cables assembling at the edge, while inhibition of muscle contraction (menthol) has no major effect. Controls: FASW (filtered artificial sea water), DMSO, Ethanol. **(B)** Menthol efficiently blocks muscle contraction in undissected and bisected jellyfish. Note that jellyfish contract significantly faster after amputation. Number of contractions per minutes recorded for 5 minutes for 10 undissected and newly bissected jellyfish, in control (0,04% ethanol) and menthol (400 µM) conditions. Statistical test: Mann Whitney Wilcoxon. **(C)** Myosin phosphorylation in intact and remodeling fibers. Myosin phosphorylation can be detected in radial smooth muscle fibers (central and peripheral umbrella) but not in circular striated muscle fibers (peripheral umbrella only), negative control (Ilr rho) also shows no staining. Disorganizing muscle fibers (6 hpd) are instead accompanied by myosin phosphorylation, and show enhanced contractility. Scale bar: 25 µm.